POLITECNICO
MILANO 1863

SCUOLA DI INGEGNERIA INDUSTRIALE
E DELL'INFORMAZIONE

Executive Summary of the Thesis

Development of a Perovskite-based interface for biophysical studies

Laurea Magistrale in Engineering Physics - Ingegneria fisica

Author: Francesco Strata

Advisor: Prof. Guglielmo Lanzani

Co-advisors: Prof. Fabrizio Pirri, Dr. Sara Perotto

Academic year: 2020-2021

1. Introduction

The use of light for the stimulation of living cells and tissues has recently opened a wide range of possible applications in biology, medicine, and robotics [1]. The typical targets of this approach are neurons, due to their prominent role in signal processing and control, or muscle cells for addressing light-controlled movement. In the last decade, control of neuronal paths or vital functions by means of light-based stimuli, simply referred as photostimulation, has effectively emerged as a valid alternative to the electrical counterpart. Among the great advantages of choosing photostimulation, there are the inherent high resolution and selectivity properties of light, the avoidance of physical contact between the stimulation source and the target, and the possibility to decouple the recording and stimulation phase.
However, living cells do not generally possess any specific sensitivity to light. Artificially inducing light sensitivity to cells is therefore the primary goal of researches in the field of photostimulation. Several methods have been developed to this purpose, but no one has emerged as the winning solution yet. One of the most promising approaches to photostimulation is the use of an external phototransducer, a system able to elicit a cellular response by means of light excitation. Final aim of this project is to understand the photo-biological phenomena at the biotic-abiotic interface by exploiting photostimulation. This thesis work is focused on the fabrication, characterization and modelling of opportunely designed substrates. To this purpose, the possibility of using a perovskite-based interface as suitable phototransducers for the study of stimulation of living cells has been explored.

2. Methods

The final goal of this work is to study the interaction of the biotic-abiotic interface exploiting the outstanding optical properties of perovskite materials, which guarantee wider spectral range response and higher efficiency with respect to other phototransducers. In particular, methyl ammonium lead iodide ($CH_3NH_3PbI_3$), namely MAPI, was selected among the other metal halide semiconductors. Given its archetypal nature, this perovskite crystal has been widely explored in its features, both in terms of chemical structures and optical properties [2]. Together with other halide perovskites, MAPI is a standard photoactive absorber in photovoltaics. In fact, it possesses excellent optical properties that have been widely exploited for visible light op-

toelectronic applications. It can be classified as an intrinsic semiconductor with direct bandgap, exhibiting remarkable mobility of both photogenerated electrons and holes. Beside the exceptional absorbing properties, MAPI has also a peculiar defect-tolerant nature.
As a downside, perovskite materials suffer from deterioration and instability when exposed to external agents. Four are the principal factors that affect metal halide perovskites behaviour altering their intrinsic physics [3]: (i) moisture and, in general water; (ii) oxidation; (iii) photodegradation; (iv) thermal stress. Therefore, due to the inherent fragile stability of this kind of materials, samples require a careful and systematic preparation in order to avoid any contact between MAPI's compounds and possible degrading agents, notably water, which is the main component of biological tissues and cellular environment. Given the novelty of this employment of perovskites, samples were necessarily fabricated ex-novo and opportunely engineered to be interfaced with biological environment in *in vitro* experiments. A deep characterization of the fabricated devices and their optical properties was a fundamental step towards the main objective.

2.1. Fabrication

In this study, since the scope was not to obtain a particularly efficient device for photovoltaic applications, a standard protocol based on photovoltaic cells manufacturing techniques has been followed, to obtain a relevant quality in terms of optical properties that justifies the use of perovskites for photostimulation purposes. The first step to move towards fabrication of thin films is the preparation of the substrate. Indium-tin-oxide (ITO) coated glasses were cleaned with acetone and IPA and treated for the subsequent spincoating with UV-Ozone. Then, methylammonium lead iodide (MAPI) thin films were spincoated (at 4000 rpm for 30 s) using the so called *anti-solvent technique*, in a clean environment, starting from a precursor solution of lead(II) iodide and methylammonium iodide in dimethylformamide (DMF)/ dimethyl sulfoxide (DMSO) $0,5$ M. After spincoating, samples were left on a hot plate at 100°C for ten minutes to evaporate the solvent. Samples were then coated with an organic semiconductor (OSC), chosen between Spiro-OMeTAD (SPIRO) and Phenyl-C61-butyric acid methyl ester (PCBM). The first is one of the most suitable hole transport layer materials (HTL), whereas the second is often used in organic solar cells as an electron acceptor or electron transport layer material (ETL). The OSC coating was performed by spin coating at 2000 rpm for 30 s. The spincoating parameters were adjusted to obtain a film thickness of approximately 150 nm for MAPI and 200 nm for the OSC layer. At the end, the multilayer substrates manufactured were similar to typical solar cells, where the nature of the OSC allowed to selectively accumulate positive/negative charges at the interface.

2.2. Passivation

Ensuring long-term stability of metal halide perovskite semiconductors is one of the most challenging task in the field of solar cells development and hence the great limit for effective applications of these materials. In particular, since the materials in question are salts and take on water very easily, a uniform thin passivating layer sufficient to protect the perovskites from infiltration for the minimum time needed for *in-vitro* experiments is required. In order to fulfill this severe requirement a Parylene conformal deposition by means of CVD (Chemical Vapor Deposition) was chosen as the winning solution. This process has a large number of advantages since it provides a systematic and high-value surface treatment with excellent moisture, chemical and dielectric barrier properties by means of a ultra-thin, biocompatible polymer coating. By lowering the deposition pressures, and therefore the deposition rate, the conformal nature of the parylene coating was exploited at its best. A deposition between 7 and 8 $mtorr$ was employed for this purpose. Different thicknesses were tested, from 1 μm to 200 nm.

2.3. Optical Characterization

A schematical picture of the final substrate structure is reported in Figure 1. The result was a glass/ITO substrate where a MAPI thin film and an optional OSC layer lay upon, all encapsulated by an insulating and water-resistant layer of polymer. This type of sample had to be validated at each crucial step of realization, especially evaluating the stability of the

optical-responsive materials in response to ambient condition and, above all, presence of water. Absorbance spectrum and XRD measurements were collected to monitor the status of the sample. The first allows to verify photoabsorbing properties of the material, while the second monitors the crystalline structure of the perovskite layer. In particular, a MAPI crystal is expected to have the main characteristic peaks at 14.1° ((110) principal plane) and at 28.4° ((220) principal plane).

Figure 1: Schematic of the samples.

2.4. Electrochemistry

Electrochemical characterization served as important tool to verify the optoelectronic behaviour of encapsulated perovskites in presence of wet environments, preceding the exposition to cells. These experiments have been conducted using potentiostatic and galvanostatic measurements and a three electrode electrochemical cell setup. The Metrohom PGSTAT302N equipment was used, together with a Pine Research RRPG147 quartz photoelectrochemical cell. The cell was arranged in a way that ITO-side of the thin film could be exposed to a light of a LED and the other side, the encapsulated one, could be interfaced with an electrolytic solution. One edge of the samples was carefully cleaned with acetone to permit the electrical contact with the ITO substrate, which was thus connected with the working electrode (WE) through a crocodile clip. Then, a saturated $Ag/AgCl$ (Metrohm 60733100) was used as RE, while a Pt wire (Metrohm 60301100) was used as counter electrode. Both were drawn in the electrolytic solution and close the circuit. The solution was a 200 mM $NaCl$ solution in $Milli-Q$ water and not pH-adjusted. The light, instead, was supplied by a green LED (Thorlabs M530L3-C5) working at 530 nm and driven by a DC2200 LED digital driver. The LED was placed at 25 cm from the sample and operated at maximum power, with a resulting intensity of light impinging on the sample of 500 W/m^2. A very similar arrangement had already been used in a previous study to obtain a quantitative description of the fundamental mechanisms related to the photoactivation of P3HT thin films [4]. Photovoltage and photocurrent experiments were conducted. Data were acquired for 5 seconds, while a light pulse of 500 ms illuminated the ITO-side of the sample. Instrument resolution reached 10^{-4} s.

3. Results and discussion

3.1. Substrate encapsulation

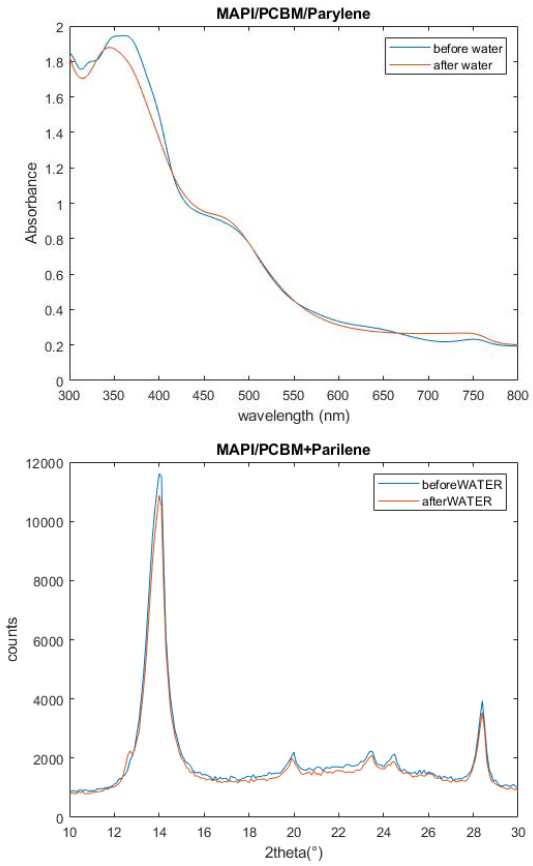

Figure 2: XRD and absorbance spectrum measurements showing the preservation of the crystalline structure and the absorbing properties of the substrates.

In the experimental validation, the first point was to make sure that polymer layer was not altering the underlying substrate. This was confirmed by XRD. The only effect of parylene is to marginally enlarge the width of the characteristic peaks. The possible explanation for that is believed to be due to X-ray scattering from the polymer structure which, as a result,

gives a convoluted peak.

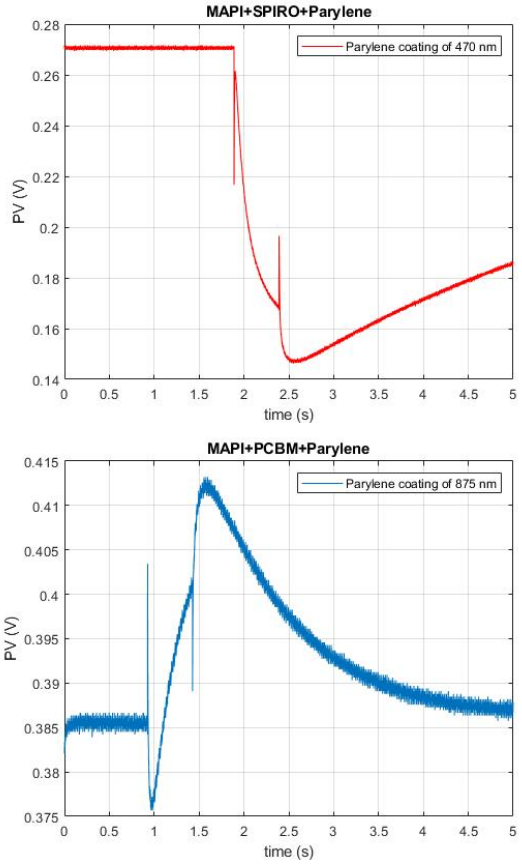

Figure 3: Two photovoltage measurements of SPIRO (on the top) and PCBM (on the bottom) coated samples. Importantly, the behaviour is of opposite sign according to the OSC layer present in the sample, as expected by the different charge carrier extracted.

Then, the substrate was subjected to a series of stressing tests in order to effectively prove its stability in atmosphere and physiological environments. Specifically following these steps:

1. exposure to air for 24 hours (previosluy stored in vacuum conditions);
2. thermal annealing (hot plate at 100°C for 2 hours) to simulate the sterilization step;
3. exposure to water for 4 hours.

Absorbance spectrum and XRD measurements were taken before and after the treatments (Figure 2). The former showed a practically preserved spectrum, while XRD proved the maintenance of perovskite characteristc peaks. Thus, the results showed that the employed encapsulation is an effective way to prevent perovskites films from air, heat and aqueous environment for several hours.

3.2. Electrochemical characterization

The last step before approaching the phototransducing substrate to cells was an electrochemical characterization. These measurements allow to model the interaction between the optoelectronic system and the electrolyte, giving insights for the possible behaviour once in contact with cells.

Photovoltage In Figure 3 the representative traces of photovoltage measurements are shown. In essence, the traces show two types of sample's behaviour: (i) a very fast peaked trend given by electronic effects at the light on-off moments, and (ii) a much slower voltage shift due to a reaction of the system to the impinging light. It is important to say that the former can be resolution-limited, since the electronic time constants can likely be faster than the instrument resolution (10^{-4} s). For this reason, the amplitude of the peaks is probably higher than the one collected by the measurement. Moreover, light-ON and light-OFF peaks are asymmetric both in sign and amplitude.
Once the light stimulus is turned off, the system reaches the equilibrium with a characteristic time that ranges from tens of seconds to several minutes. This last behaviour, also called *self-healing*, is typical for perovskites, and has been deeply investigated in literature [5]. The authors attribute this velocity asymmetry in the rise and decay of the photovoltage profile to ion migrations in the perovskite crystal.

Photocurrent Photocurrent measurements were conducted in the same condition as photovoltage acquisitions. In Figure 4, the representative traces that correspond to the same samples of the previously displayed photovoltages are reported. As for the photovoltage curves, a peaked on-off behaviour is distinguished from a slower trend experienced during illumination. Here, the measurable effects during illumination are at least a third compared with the peaks of current immediately after the LED switches, not counting the possible data loss due to limited resolution. This suggests a 'capacitive' behaviour of the system in terms of current. In particular, the steady state

photocurrent, as expected, has been apparently cut down by the insulating layer of parylene.

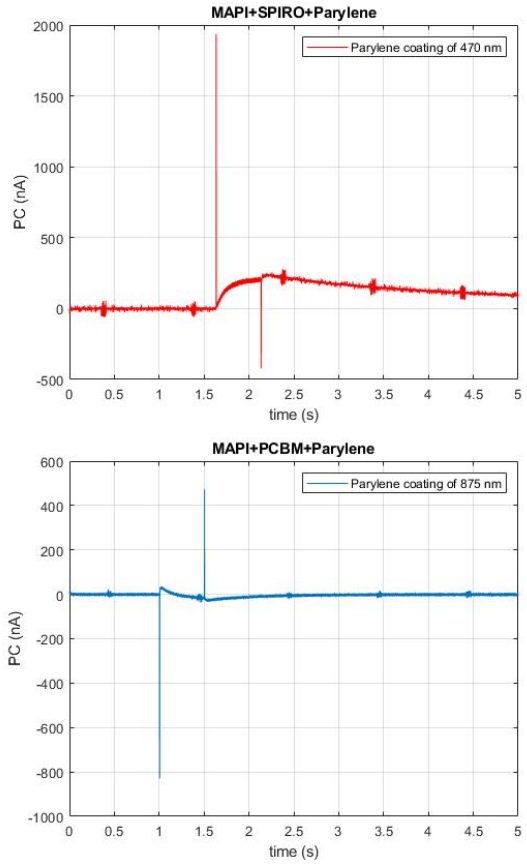

Figure 4: Photocurrent measurements of SPIRO (on the top) and PCBM (on the bottom) coated samples. As for the photovoltage, the different signs of the on-off peaks according to OSC involved are a clear indication of the different carrier involved in the extraction of charges.

3.3. Model and Simulations

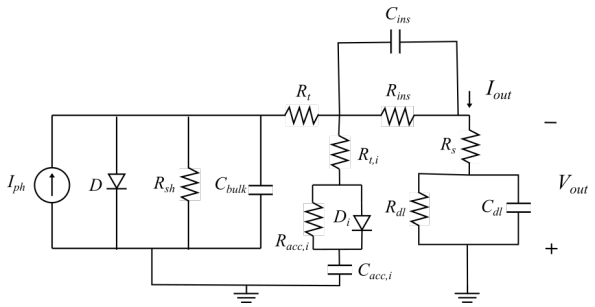

Figure 5: Schematic of the circuit model proposed.

Equivalent Circuit To better interpret the observed electrochemical behaviour of the system, an equivalent circuit model has been draft (Figure 5). In particular, the scope was to have a reliable model of the response of the sample under light stimulation, discriminate the processes involved and, maybe, identify the parameters that mostly affect the optoelectronic behaviour when interfaced with an electrolyte.
The circuit was the assembly of some recognized models for the various parts of the sample and its interaction with the electrolyte. Ideally, the substrate composed by the glass with ITO, the perovskite thin film and its OSC layer can be modeled as a solar cell and its equivalent circuit. Beside the current generator that models the photogenerated carriers, the diode stands for the junction behaviour of the solar cell, R_{sh} represents all the ohmic losses of the cell, R_t the transport resistance, and C_{bulk} all the capacitive effects generated by the various interfaces between materials and contacts. This is a standard model for the solar cell equivalent. Instead, $R_{t,i}$, $R_{acc,i}$, D_i, and $C_{acc,i}$ form a circuit branch that serve as model for the self-healing process. The $R_{t,i}$ stands for the ion transport, $R_{acc,i}$ models the highly resistive barrier for recombination, while D_i and $C_{acc,i}$ replicate the ion-induced junction generated by the polarization of charges, which caused the asymmetry in the relaxing time of the system. C_{ins} and R_{ins} are the elements for the representation of the insulating effects given by the parylene layer above the cell, which, for the setup used, must be put in series since are directly in the electrical path of the circuit. Of course, the better the electrical insulation, the higher R_{ins}. Finally, the interface between the sample, the solution and the electrode that closes the circuit (CE) is modeled with a simplified version of the *Randles circuit*. R_s is a series resistance that models the conductivity of the solution and the electrode, while C_{dl} and R_{dl} stand respectively for capacitive and faradaic coupling of the electrode/electrolyte interface.

Simulations In order to properly validate the model proposed, numerical simulations were conducted. LTspice has been used as analog electronic circuit simulator software. The circuit draft was imported in the software environment and a transient analysis has been performed to emulate the experiment conditions. Typical parameter values were taken from literature both

for the perovskite-based solar cell [5] and the electrode/electrolyte interface [6]. The results of the simulation roughly replicate the main features of the experimental data (Figure 6, Figure 7). The capacitive peaks with their opposite signs are predicted, both for photovoltage and photocurrent, together with the steady state behaviour. As expected, the slow relaxation time is also well described by the model. Interestingly, the model gives information about the origin of the experimental measurements: the *RC* constant of the insulating layer of parylene is surely the major responsible for the capacitive behaviour of the system, since the insulator cuts down the steady state component of the signal. Then, the dynamic response of the solar cell is mainly affecting the amplitude and the width of the capacitive peaks. The slower behaviour of the signals, instead, is dominated by the coupling processes of the sample with the electrolyte, that is the Randles circuit's parameters.

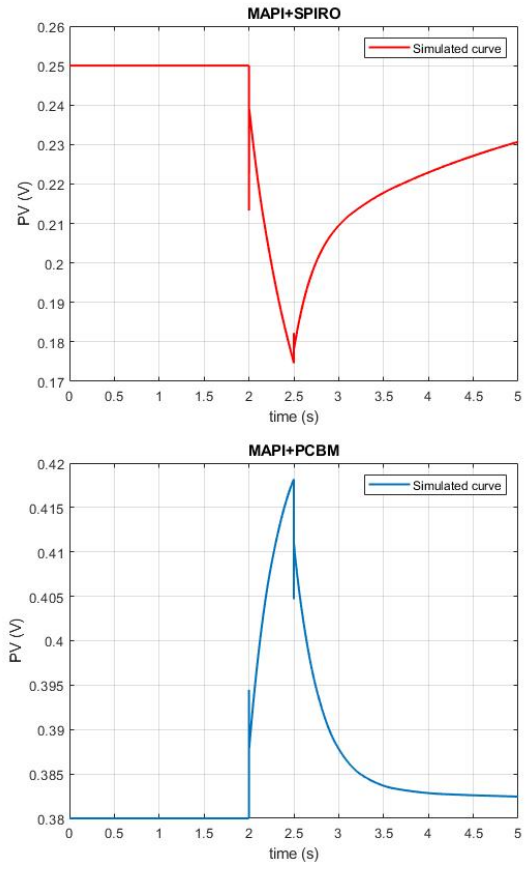

Figure 6: Simulated photovoltage for SPIRO (on the top) and PCBM (on the bottom) substrates.

4. Conclusions

The final purpose of this thesis work was to move some steps towards the understanding of the light-driven stimulation of living cells without the use of invasive nor detrimental methods. In this direction, the realization of efficient semiconductor-based phototransducers for light stimuli would be an important milestone.

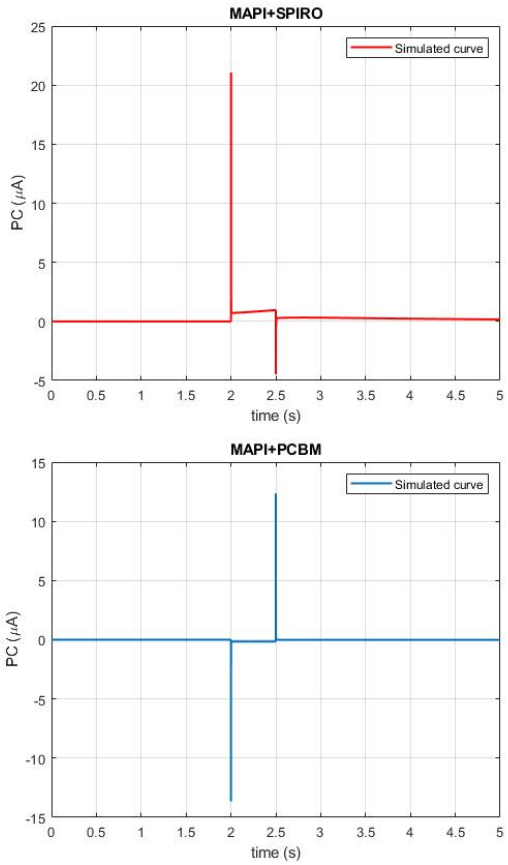

Figure 7: Simulated photocurrent for SPIRO (on the top) and PCBM (on the bottom) substrates.

First of all, a perovskite archetype crystal ($CH_3NH_3PbI_3$) has been employed as the raw material for the preparation of solar cell-like substrate. In terms of stability issues, this study has proven that chemical vapor deposition of Parylene C could be a promising method to encapsulate such substrates while ensuring biocompatibility. Importantly, the parylene thickness seems not to be a crucial parameter in the protective action against external agents. While, the compactness and the uniformity of the coating has been shown to be the key for a successful encapsulation.

Then, electrochemistry measurements have been conducted to simulate the response of the system in a physiological environment. These measurements have shown the presence of a peaked electronic response at the light switching moments, suggesting a capacitive charging and discharging behaviour. At the same time, the steady state behaviour of the system seems not to be completely cut down by the insulating action of the parylene polymer. An equivalent circuit model has been also developed to properly interpret the results from electrochemistry. Transient simulations performed with LTspice have been conducted to replicate the experimental conditions and validate the model proposed. The model succeed in predicting the capacitive peaks both in SPIRO and PCBM coated substrates, suggesting that the electrical properties of the insulation layer are the controlling parameters for such behaviour. The natural evolution of this study is to validate the biocompatibility of these substrates for *in-vitro* experiments. Then, the eventual response of cells to the optoelectronic coupling provided by such substrates has to be further studied and interpreted. This future activity will hopefully shed light on the coupling mechanisms of cell excitation related to the plasma membrane.

References

[1] Francesca Di Maria, Francesco Lodola, Elena Zucchetti, Fabio Benfenati, and Guglielmo Lanzani. The evolution of artificial light actuators in living systems: from planar to nanostructured interfaces. *Chemical Society Reviews*, 47(13):4757–4780, 2018.

[2] Ajay Kumar Jena, Ashish Kulkarni, and Tsutomu Miyasaka. Halide perovskite photovoltaics: background, status, and future prospects. *Chemical reviews*, 119(5):3036–3103, 2019.

[3] Caleb C Boyd, Rongrong Cheacharoen, Tomas Leijtens, and Michael D McGehee. Understanding degradation mechanisms and improving stability of perovskite photovoltaics. *Chemical reviews*, 119(5):3418–3451, 2018.

[4] Greta Chiaravalli, Giovanni Manfredi, Riccardo Sacco, and Guglielmo Lanzani. Photoelectrochemistry and drift–diffusion simulations in a polythiophene film interfaced with an electrolyte. *ACS applied materials & interfaces*, 13(30):36595–36604, 2021.

[5] Firouzeh Ebadi, Masoud Aryanpour, Raheleh Mohammadpour, and Nima Taghavinia. Coupled ionic-electronic equivalent circuit to describe asymmetric rise and decay of photovoltage profile in perovskite solar cells. *Scientific reports*, 9(1):1–9, 2019.

[6] Jun-Uk Chu, Kang-Il Song, Ahnsei Shon, Sungmin Han, Soo Hyun Lee, Ji Yoon Kang, Dosik Hwang, Jun-Kyo Francis Suh, Kuiwon Choi, and Inchan Youn. Feedback control of electrode offset voltage during functional electrical stimulation. *Journal of neuroscience methods*, 218(1):55–71, 2013.

Politecnico di Milano

SCUOLA DI INGEGNERIA INDUSTRIALE E DELL'INFORMAZIONE

Laurea Magistrale – Engineering Physics

Development of a Perovskite-based interface for biophysical studies

Relatore

Prof. Guglielmo LANZANI

Co-Relatore

Prof. Fabrizio PIRRI, Dr. Sara Perotto

Candidato

Francesco STRATA – 944491

Anno Accademico 2020 – 2021

Ringraziamenti

Per prima cosa, ringrazio il CNST-IIT che ha ospitato gran parte dell'attività sperimentale e reso possibile la realizzazione di questo progetto. Ringrazio inoltre i miei relatori per la loro paziente attenzione nei miei confronti e i preziosi suggerimenti di cui spero di aver fatto tesoro.
Questo elaborato va a suggellare il termine di un percorso durato due anni, fatto di passione, determinazione e coraggio, ma anche di sacrifici, sudore e rinunce. Il mio obiettivo era quello di imparare sempre, da tutti e da tutto ciò che si poneva sul mio cammino. E si sa, si impara di più nei momenti difficili, quando la strada è in salita, che quando si vive nella comodità.
Ringrazio chi da lassù non si è mai dimenticato di me e chi, da quaggiù, non mi ha mai fatto mancare il suo sostegno.
Grazie ai miei genitori, che mi hanno insegnato ad essere tenace e a non lasciare mai spazio alla rassegnazione.
Grazie agli amici, che con la loro solidarietà e il loro operoso affetto hanno reso tutto più semplice.
E una speciale dedica a te, Eleonora, che hai reso la mia vita più luminosa. D'altronde, la luce è stata l'oggetto dei miei studi e di questa tesi di laurea, ma del tuo chiarore ho sempre avuto bisogno.

Sommario

L'impiego della luce come sorgente di stimolazione per cellule e tessuti ha recentemente generato un ventaglio di promettenti applicazioni in biologia, medicina e robotica. Nell'ultimo decennio, infatti, il controllo delle vie neurali o delle funzioni vitali per mezzo di stimoli luminosi, definito spesso semplicemente come fotostimolazione, è emerso come potente alternativa alla stimolazione elettrica, per i suoi notevoli vantaggi in termini di invasività, risoluzione temporale e spaziale. Tuttavia, siccome le cellule in genere non possiedono particolare sensibilità alla luce, indurre artificialmente questo tipo di sensibilità è senza dubbio il primo obiettivo di tutte le tecniche di fotostimolazione.
In questo studio, substrati di film sottili di perovskite sono stati proposti come fototransduttori esogeni in grado di tradurre l'eccitazione luminosa in un appropriato segnale per le cellule. L'archetipo perovskitico $CH_3NH_3PbI_3$ è stato scelto come materiale fondamentale per la preparazione di substrati con il comportamento simile a quello di una cella solare. Inoltre, la deposizione conforme di uno strato di Parylene C è stata proposta come metodo di passivazione delle perovskiti, rivelandosi promettente. Quindi, il substrato incapsulato dal polimero è stato sottoposto ad esperimenti di elettrochimica per verificare il suo comportamento in un ambiente che replicasse le condizioni fisiologiche. Un modello di circuito equivalente è stato sviluppato per interpretare meglio i risultati sperimentali. Le simulazioni LTspice hanno confermato in buona parte la validità del modello aiutando a comprendere meglio alcuni aspetti dei fenomeni elettrochimici.
I prossimi passi di questa attività di ricerca saranno naturalmente quelli di verificare l'effettiva biocompatibilità dei fototransduttori proposti e studiare l'eventuale risposta delle cellule. Quest'ultima analisi sarà auspicabilmente una pietra miliare importante per una comprensione più profonda dei meccanismi di accoppiamento che regolano l'eccitazione cellulare.

Abstract

The use of light for the stimulation of living cells and tissues has recently opened a wide range of possible applications in biology, medicine, and robotics. In the last decade, control of neuronal paths or vital functions by means of light-based stimuli, simply referred as photostimulation, has effectively emerged as a valid alternative to the electrical counterpart. Yet, since living cells do not generally possess any specific sensitivity to light, artificially inducing light sensitivity to cells is the primary goal of photostimulation techniques.
Here, perovskite-based substrates are proposed as an external phototransducer that translates the light excitation in a proper signal for the cells. A perovskite archetype crystal ($CH_3NH_3PbI_3$) has been selected as the raw material for the preparation of solar cell-like substrate, given its outstanding optical properties. Then, chemical vapor deposition of Parylene C has been proven as a promising biocompatible alternative to standard inorganic passivation techniques. The compactness and the uniformity of the coating has been shown to be the key for a successful encapsulation, rather than thickness. The so obtained substrate were tested with electrochemical measurements to assess the response of the system in a condition similar to a physiological environment. Also, an equivalent circuit model has been developed to properly interpret the results from electrochemistry. Hence, transient simulations performed with LTspice have been conducted to replicate the experimental conditions and validate the model proposed. The model has been demonstrated to be in good agreement with the experimental results and was useful for the interpretation of the system behaviour.
The natural evolution of this study is the approach to cell culture to validate the compatibility of the explored substrates with life. Then, the eventual response of cells to the optoelectronic coupling provided by such substrates has to be further studied and interpreted. This future activity will hopefully shed light on the coupling mechanisms of cell excitation related to the plasma membrane.

Contents

List of Figures

List of Tables

Introduction

Light is responsible for all life. It is the most important resource for all living organisms, it produces the air we breath through plants, it governs weather, it provides warmth and it even regulates the mood. In recent years we have learnt not only to love light but to need light. Nowadays light is exploited in the technologies of daily life; from electronical devices and the Internet to medical instruments, LED lighting, and solar cells. All are possible because of photonics. Moreover, scientists have newly understood that the application of light have a great potential also in life sciences. In particular, the use of light for the stimulation of living cells and tissues has recently opened a wide range of possible applications in biology, medicine, and robotics [10]. The typical targets of this approach are neurons, due to their prominent role in signal processing and control, or muscle cells for addressing light-controlled movement. In the last decade, control of neuronal paths or vital functions by means of light-based stimuli, simply referred as photostimulation, has effectively emerged as a valid alternative to the electrical counterpart. Among the great advantages of choosing photostimulation, there are the inherent high resolution and selectivity properties of light, the avoidance of physical contact between the stimulation source and the target, and the possibility to decouple the recording and stimulation phase. However, living cells do not generally possess any specific sensitivity to light. Artificially inducing light sensitivity to cells is therefore the primary goal of researches in the field of photostimulation. Several methods have been developed to this purpose, but no one has emerged as the winning solution yet. One of the most promising approach to photostimulation is the use of an external phototransducer that translates the light excitation in a proper signal for the cells. This thesis work is therefore focused on this last way to photostimulation. The ultimate objective is to clear out the obscurities still present in the different coupling phenomena between light and the biological materials, in order to maximize the benefits of photostimulation. To this purpose, perovskite crystals were selected as valid candidates for the role of photoactive materials given their outstanding optical properties. Hence, the possibility of using perovskite as suitable phototransducers for the study of stimulation of living cells has been explored.
In the first chapter the principles of photostimulation are briefly reviewed, together with some fundamentals of the cell physiology. Then, the properties of perovskite materials were analyzed, focusing on their advantages and disadvantages and on the possibility of their employment in biological environments. Lastly, in the third and fourth chapters the experimental activity is presented, starting form the materials and the methods employed to the analysis and discussion of the collected data.

Chapter 1

Fundamental Principles of Photostimulation

Recent advances in all scientific fields have made possible a deeper and deeper interaction between living nature and human technologies. Yet, the language spoken by biology is often very different from the one spoken by technologies such as electronic devices and the coexistence between the two worlds has never been so easy to be put in practice, especially at microscopic scales. Disciplines such as biophysics and bioelectronics have answered to this need by putting together the knowledge of biology, optics, electronics, electrochemistry and medicine, thus giving birth to an innovative interdisciplinary field with the aim of improving diseases knowledge and treatment. Prominent examples of this approach are already common in many sectors such as robotics, prosthesis, brain/machine interfaces, and nanomedicine [11]. The ability to interface an artificial device with a living system is fundamental to achieve an efficient and controllable communication between the biological and electrical signals via biocompatible and functional materials. Recording, transduction and stimulation of various signals are therefore among the core goals of a typical bio-interface. In particular, stimulation of living cells is one of the most appealing field of research since the first experiments by Luigi Galvani with frog nerves back in the 18th century. The first approach to cellular excitation was based on injection of electrical charges through electrodes and is still widely employed both in functional therapies and neuroscience [12] [13]. However, along with the recent advancements in optics and photonics, the idea of a light-based manipulation of cell activity has recently caught on. In particular, photostimulation is able to address the key limitations of the electrical counterpart, lowering invasiveness while increasing spatial and temporal resolution, thus opening groundbreaking opportunities for selective, wireless and powerless stimulation.
Studying more thoroughly the process of photostimulation of cells is the ultimate goal of this study. Hence, the following chapter is dedicated to a brief review of the fundamental knowledge of topics related to photostimulation, from the biological target fundamentals [1], to the known methods and the current research.

1.1 Physics of the biological target

Apart from methods that trigger a unique cell type or a specific part of it, photostimulation techniques generally use less selective phototransducers with the possibility of targeting a broad variety of tissues. In this sense, the actual target of the stimulation ought to be considered the plasma membrane, thanks to its almost universal composition. For this reason, a thorough understanding of membrane structure and properties is strongly recommended when approaching this field of research.

1.1.1 Membrane structure and Properties

Each cell is bounded by a membrane which is about 5 nm thick. This membrane has many important properties, but for the purposes of this study two are of particular interest. First, it is selectively permeable; which means that it allows some molecules to pass across it (into or out of the cell) more easily than others. Secondly, it is also capable of active pumping of substances from the outside medium into the cell. These mechanisms regulate the intracellular environment, by which the membrane controls the chemical processes and the cellular activity. The cell membrane is mainly constituted by lipids and proteins. Lipid molecules consist of a polar headgroup to which is attached one or two long hydrocarbon tails. The hydrocarbon tails of the molecule tend to avoid coming into contact with water molecules, because of their hydrophobic nature. In turn, the polar head is hydrophilic and prefers to stay in contact with the aqueous environment. In water, the common feature of lipids is the fact that the hydrocarbon tails congregate together to protect themselves from contact with the aqueous medium, forming ordered structures. In cell membrane, the lipid molecules are found to be arranged in a typical bilayer as illustrated in Figure 1.1. The bilayer is a stable structure since a surface of this nature successfully protects the hydrophobic lipid tails from the aqueous phase.

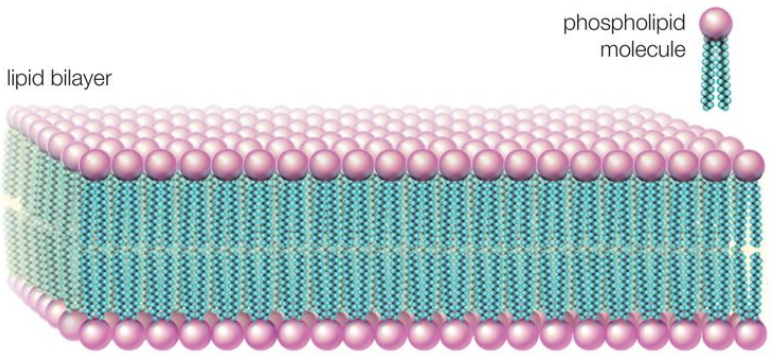

Figure 1.1. Phospholipid bilayer arrangement in a cell membrane.

Proteins, instead, are placed within the membrane in long unbranching chains of

amino acids folded into an immense variety of shapes and sizes. Amino acids are characterised by their different side chains which may be hydrophilic or hydrophobic. Proteins are characterized by highly selective properties, which are determined by the sequence of over 20 different amino acids in a chain made of about 100 amino acids per chain, so that the number of possible configurations is immense. Membrane proteins can be divided in two main categories, according to their arrangement in the membrane structure: the ones that are strongly anchored to the membrane, the so called *intrinsic membrane proteins*, and the ones that are attached with non-covalent interactions and can be gently extracted from the membrane: the *extrinsic* or *peripheral membrane proteins* (Figure 1.2). Some membrane proteins are essential

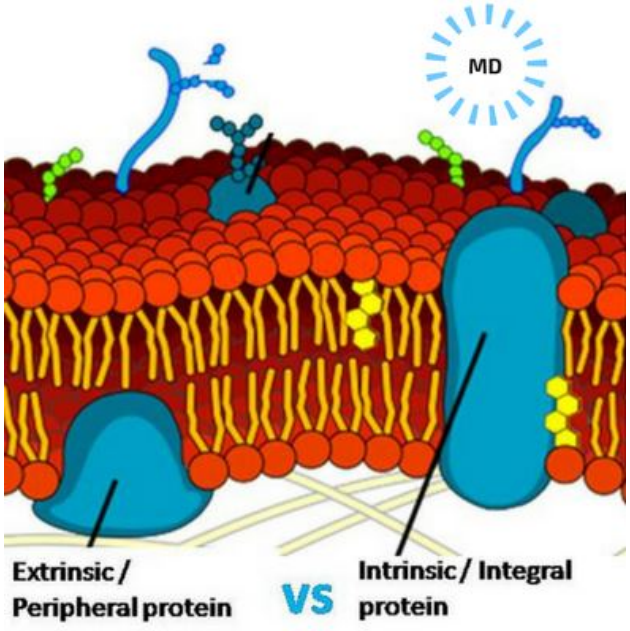

Figure 1.2. Schematic difference between intrinsic and extrinsic membrane proteins.

components of any excitable cell. In particular, the ones engaged on active transport of ions, also called *ion pumps*, use chemical energy to permit ion movement against *electrochemical gradient*, that is moving species from regions of low concentration to regions of high concentration. Sodium pump is the most famous example [1]. The alternative mechanism of transport across the membrane is due to the selective passive ionic permeabilities. Constant ionic permeability belongs to this second type. It is not affected by physiological stimuli and is also termed *resting permeability*. The primary permeability regards potassium [1].
Indeed, another passive mechanism of permeability is present in cells. This further process is not constant but may change rapidly due to the action of a stimulus. For this reason, it is said to be 'gated' by the stimulus and is the crucial characteristic of excitable membranes. One of the most important gating mechanisms is the one associated to nerve membranes. Here the protein structure is charged so that the ions are prevented electrostatically from entering the pore until a voltage stimulus across the membrane is able to 'open the gate' (Figure 1.3). Anyway, other types of gating are thought to be employed by the cell membrane. The opening and closing loop could be sensitive to chemical binding, mechanical deformation and perhaps even

to light.

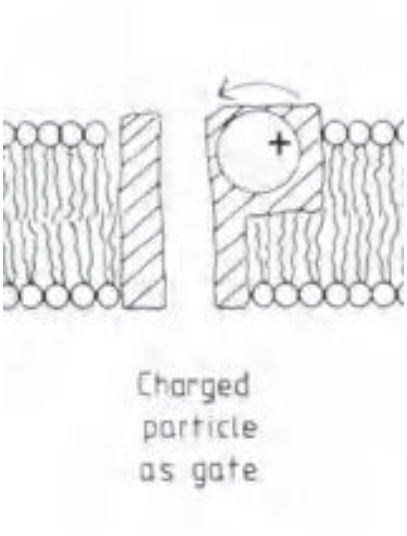

Figure 1.3. Schematic of a gated protein in a cell membrane [1].

1.1.2 The basis of Excitability

The excitable cell membrane mainly works thanks to its selective permeability to ions, even though numerous studies of the permeability properties of the pure lipid bilayer have been performed [14]. As predicted from its structure, the bilayer is highly impermeable to ions. This is basically due to the fact that (i) the transfer of a water-soluble ion into hydrophobic tails is energetically unfavourable and (ii) the presence of the so called *image potential barrier*. The latter prevents an electric charge from moving towards a low dielectric medium when it is close to a conducting high dielectric medium - the aqueous environment. Conversely, the bilayer permeability to water is much higher than that to ions as the image potential barrier is not encountered by a neutral molecule. Yet, water flux across the bilayer is consistently inhibited by the unfavourable transfer of a water molecule into the membrane interior [1]. Since the contribution of the bilayer to permeability appears to be restrained, membrane proteins are the actual responsible for ion transport. For a clearer comprehension of the relation between ion permeability and cell excitation one has to refer to the *electrochemical gradient*. The electrochemical gradient is a measure of the force driving passive flux of an ion into or out of the cell membrane. The membrane is able to create such gradients and use them to drive cell excitability. The electrochemical gradient is composed by two components: the electrical part simply consists in the difference of the electrical potential between the inside and the outside of the cell, while the chemical component is due to the gradient of the chemical concentration between the intracellular and the extracellular fluids. The latter describes the fact that ions diffuse from regions of high concentration to regions of low concentrations. In equilibrium, considering only passive mechanisms of transport, the electrical and the chemical gradients have to be perfectly balanced. The process is ruled by the

Nernst equation:

$$V = 2.303 \frac{RT}{zF} \log \frac{C_o}{C_i} \tag{1.1}$$

where V is the voltage membrane, C_o and C_i are the extracellular and intracellular concentration of the ion, T is the temperature, while z is the ion's valency and F is the Faraday's constant. However, ion pumps in the excitable membrane have the ability to

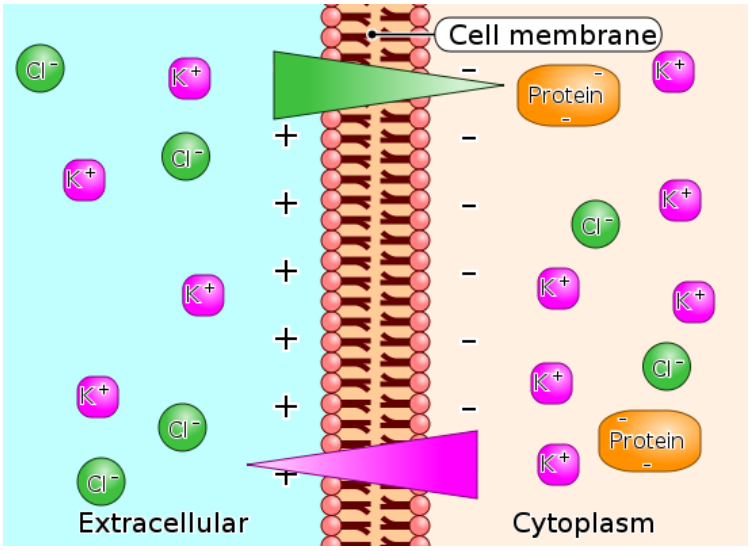

Figure 1.4. Representation of the two components of an electrochemical gradient: the coloured triangles indicate the difference in chemical concentrations of potassium and chlorine, while signs of charges indicate the electrical component of the gradient.

create and maintain ion concentration gradients by moving ions against electrochemical gradients with active transport processes. Once that an electrochemical gradient is set in this way, the membrane potential is ruled by selective passive permeability to the ion species. The ease with which an ion can cross the membrane may be quantified using the so called *membrane conductance*. For example, in the resting state of the cell there is a higher potassium conductance than sodium or calcium conductance [1]. Therefore, the resting membrane voltage is typically close to the one calculated using the Nernst equation for potassium 1.1. In fact, in the resting state of an excitable cell, sodium and calcium ions, despite large inward electrochemical driving force, enter slowly as the membrane conductance to these ions is very low. However, the so called *excitable* ion channels have the ability to rapidly change the conductance of ion species. In its simplest form, the excitable mechanism involves the opening or the closing of membrane channels to an ion mediated by a specific stimulus. These processes are depicted in Figure 1.5. The important thing to clear out is that the flow of ions through these channels are not determined by the energy of the stimulus but by the pre-existing electrochemical gradient, in particular by the membrane voltage. Another fundamental concept is the *regenerative mechanism*. Consider for example an increase in the membrane voltage which drives the opening of a sodium channel gating. The induced sodium ion flow will itself cause a further increase in membrane voltage and, by consequence, tend to open more channels. This cycle is reported in Figure 1.6.

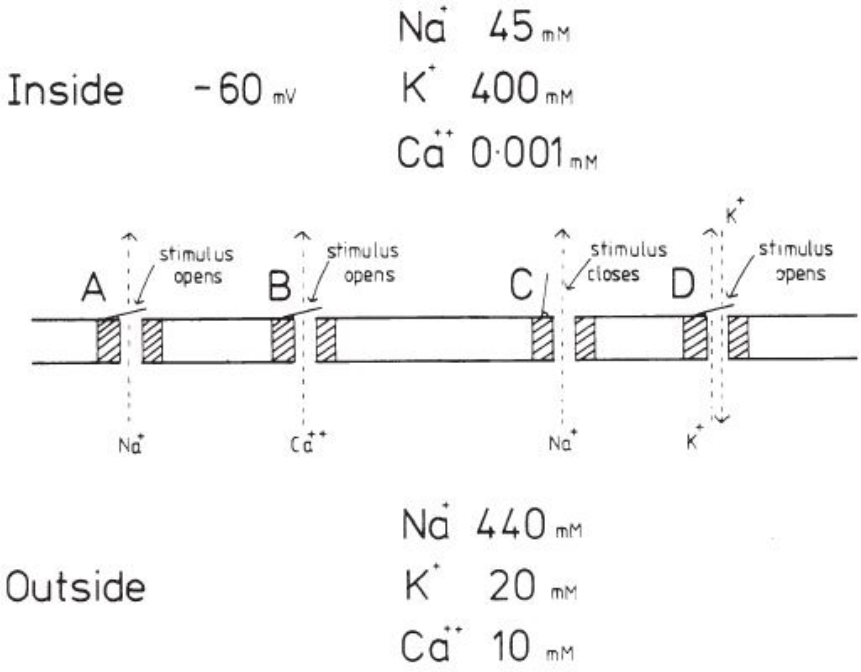

Figure 1.5. Examples of gated ion channels for sodium, calcium and potassium ions. Channels A, B, and D, permeable to calcium, sodium, and potassium, can be opened by a stimulus. Whereas, channel C is open in the resting state and the stimulus closes the gate [1].

The stimulus is said to be *self-reinforcing*, because it creates a positive feedback of amplification. Beside that, a certain threshold in terms of stimulus' strength must be reached before the regenerative mechanism can overcome the natural decay of the single channels excitation. The last concept involving this kind of critical threshold is found in many excitable tissues, and most notably in nerve cells.

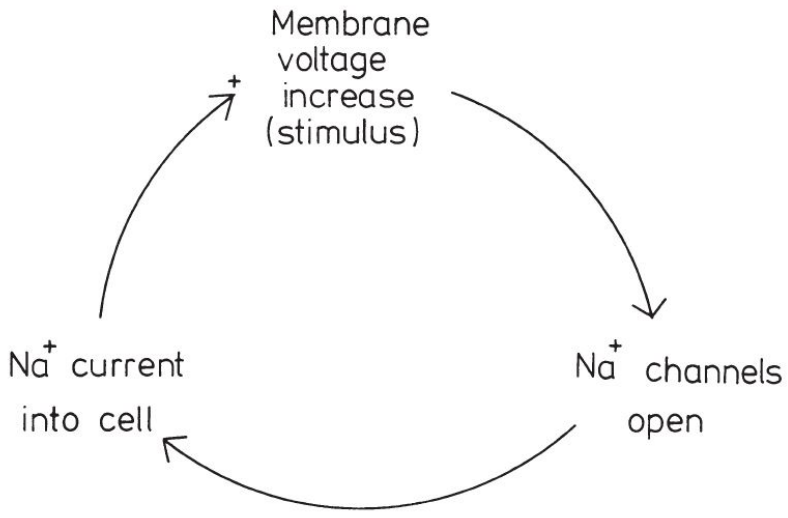

Figure 1.6. Self-regenerative cycle which amplifies changes in membrane voltage [1].

1.1.3 Cell Membrane Equivalent Circuit Model

For the purposes of this study, where an optoelectronic substrate is interfaced with living cells, light is traduced in an electrical signal which is supposed to change the electrochemical gradient nearby the cell and, therefore, influence the membrane voltage. These processes have to be further investigated and, for this reason, an appropriate electrical equivalent model for the membrane can be really useful. In particular, the dynamic response of the membrane can be described by an electrical circuit composed by a parallel between a capacitor C_m and the series of a resistance R_m and a voltage generator E_eq [2]. The capacitor models the dielectric properties of the lipid bilayer and its impermeability to ions. The double layer of lipids is expected to behave as a parallel plate capacitor whose capacitance (C) is given by the common relationship:

$$C = \frac{\varepsilon_h A}{d} \tag{1.2}$$

where ε_h is the hydrocarbon sheet dielectric constant, A is the area of the bilayer, and d the hydrophobic region thickness. Capacitance studies on cell membranes are not straightforward, but capacitance of artificial bilayer is found to be about 0.4 $\mu F/cm^2$ [1]. The resistance, instead, is used to describe the membrane conductance to ions due to opened ion channels. Eventually, the generator is the equilibrium potential difference between the intracellular and the extracellular environment: when no voltage is applied, this difference is equal to the resting potential. This simple model is a rough tool to interpret ion currents across the membrane.

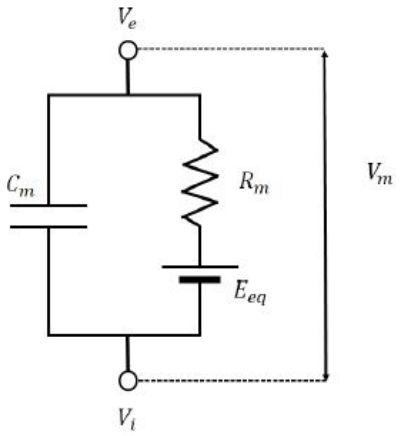

Figure 1.7. General schematic of the membrane equivalent circuit [2].

1.2 Photostimulation process and types of interaction

Once understood the main features of the biological target of stimulation, it is important to know how it can be coupled with the external stimulus, which, in the case of photostimulation, is light. Since, as anticipated, cells do not generally have particular sensitivity to light, a coupling mechanism of signal transduction is necessary

to trigger the biological activity. Primarily, the latter is strongly dependent of the nature of the phototransducer. Secondly, the biological environment and the features of the illumination source play an important role.
Also for these reasons, the mechanism that rules the stimulation of cells takes is still under debate. Yet, the main ruling effects affecting a bio-interface can be essentially described by modeling the target as an electrolyte. Therefore, three main types of stimulation mechanisms have been distinguished [3] [2]:

- the *capacitive* process is characterized by a redistribution of charges causing the generation of local, transient electric fields close to the polymer/electrolyte interface. The mechanism is called capacitive since the material/electrolyte interface can be modeled as a capacitance formed by the electrons (or holes) of the optoelectronic device in contact with the ionic double layer (DL) generated in the electrolyte to reach charge neutrality. As a result of a local charge redistribution response, a transient electric field and ionic current are produced. Thus, membrane polarization or depolarization can occur, depending on the sign of the optically generated charges.

- the *Faradaic* process is the one which involves electrochemical oxidation or reduction reactions caused by electron transfer between the polymer and electrolyte. The reactions, unlike the capacitive effect, can be either reversible or irreversible. The last case typically occurs when some reaction products diffuse away from the interface before the reverse reaction. In any case, reaction products are indeed the responsible for the interaction with the cell membrane.

- *thermal* stimulation occurs when impinging light is responsible for an increase of the temperature of the phototransducer in direct contact with the biological target. The so generated gradient of temperature makes heat propagate through the bio-interface to reach cells. The thermal process dominates over the other two mechanisms when higher light intensities and exposure times are employed. Photothermal effects are thought to affect the electrical properties of the cell membrane. These changes are commonly attributed to phase transitions of the phospholipid bilayer [15].

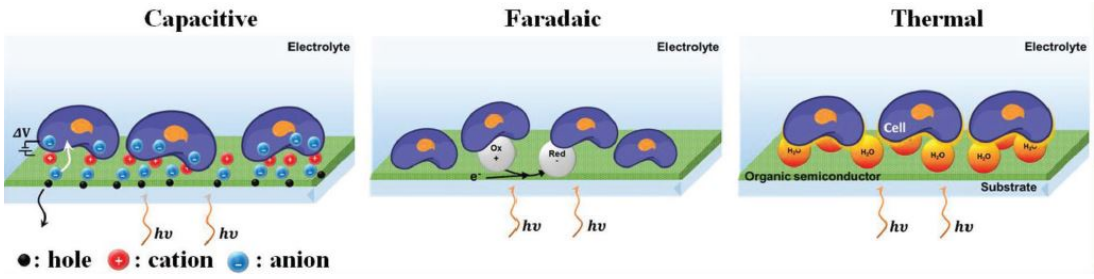

Figure 1.8. Schematic of the possible photostimulation mechanism taking place at the biological interface. Adapted from [3].

The research in the field of photostimulation has the goal to shed light on the above-listed mechanisms and typically exploit one of them to couple light with biological activity. The capacitive process is generally desired for its reversible and minimally

detrimental nature. In turn, faradaic and thermal processes have shown to be effective as well, but are limited by concerns about living tissues safety. In any case, many techniques of photostimulation have been explored, especially in the last ten years. Although each one has quite its peculiar method, techniques can be classified to a certain family, according to the approach followed. Indeed, methods to stimulate cells based on light are divided in two main categories [16]: (i) those that require photoactive mediators designed to be specific for a cell type, to be a part of it or to trigger a particular function, and (ii) those that use less selective phototransducers able to convert the light excitation into an electrical, chemical, or thermal stimulus in close proximity with the cell. The first class relies on on photoactive absorbers enclosed inside the cell, attached to the plasma membrane, or in its immediate extracellular environment and are also called also endogenous stimulation techniques. These are:

- *Direct Stimulation*: in general, if not for the presence of peculiar photoreceptors, mammalian cells have not any specific sensitivity to light. However, examples of direct optical stimulation of neuronal cells have been reported, both through near IR light [17] [18] [19], and UV pulses [20]. This method could be preferred for its inherent simplicity, but is limited by the the fact that activation is mainly due to mechanical or biochemical stress to the tissue. Nevertheless, a technique called infrared neural stimulation (INS) based on irradiation with infrared light below the threshold for tissue damage has achieved interesting results [21] [22] [23]. It is thought that the underlying working principle of INS is based on the IR light absorption by water, which generates a local heating of the sample, activating temperature-sensitive properties of the cell membrane [24] [25].

- *Photoisomerizable and Photocleavable Compounds*: photoisomerizable compounds are photo-switchable drugs made of azobenzene derivatives. They were originally applied as pharmacological manipulation of cell function and are capable of assuming either a *cis* or *trans* configuration upon light illumination at suitable wavelengths. They need UV light for *trans* to *cis*, and visible for *cis* to *trans*. The light-induced photoisomerization is an highly efficient process and has no reactive intermediates or competing reactions [26]. In the same direction of photo-switch, a strategy based on UV photochemical cleavage has been also explored [27] [28]. Photocleavable compounds, also called *caged* compounds, can be introduced near to or within the cell of interest, where a flash of light can liberate the active compound that is somehow trapped by a photosensitive cage which undergoes photolysis. Although caged compounds are by now commercially available, many limitations still remain, like the inability to reverse the process, and limited tissue penetration of UV light [16].

- *Genetic Expression of Photosensitive Probes*: one of the most powerful technique to induce light sensitivity is surely *optogenetics*. In optogenetic stimulation, a number of genetically engineered photoactivatable probes can be used to modulate the biological activity of a single cell [29]. Optogenetics is already widespread for light interaction with the nervous system in important applications [30], but the use of viruses for gene expression has brought out safety concerns (especially in humans) and the achievement of stable and controlled long-term heterologous protein expression is still a challenge.

The second class of photostimulation techniques exploits exogenous photo-absorbers, and coincides with the field of interest of this study, that is light-directed bio-interfaces. Also in this case, there are different possibilities to approach the use of light for cell stimulation:

- the use of metal or semiconducting *nanoparticles* and, in particular, *quantum dots* (QDs): QDs have a great potential in optical stimulation of cells, since impinging light generate a dipole momentum in the nanoparticle, which can elicit nearby neuronal cells. The most efficient configuration was proved to be in form of QD layers that act as a culturing substrate [31] [32]. QDs are typically limited in applications for their possible toxicity, which needs to be further investigated.

- the use of *bulk semiconductors*, which act as functional cell-culturing substrates: they can be made of both organic and inorganic materials. Typically, the inorganic choice falls on *photoconductive stimulation*, that exploits the light-induced changes of silicon conductivity. Once that silicon is deposited on a conductive substrate, an externally modulated electrical potential is applied between the underlying substrate and a reference electrode immersed in the liquid extracellular bath. Upon illumination of an appropriate wavelength and intensity, conductivity does increase [33]. An alternate photocurrent can be either generated by modulating the external bias at fixed light or varying light intenisty at a fixed potential, successfully targeting single or multiple cells independently of their position on the substrate. However, since the limited biocompatibility, the need for electrical wiring, and the presence of a potentially cell-damaging voltage bias seem to prevent inorganic substrates from *in-vivo* applications, organic counterparts have been widely explored, thanks to the growth of organic electronics [34]. Notably, organic photovoltaics seems to be a significant field to be explored in terms of biological interaction. This study is particularly centered to this type of possibility and the group of research that hosted me has been making remarkable efforts in this direction: in 2011 they reported the photostimulation of primary neurons grown on a thin film of an organic photovoltaic blend based on the conjugated polymer poly(3-hexylthiophene) (P3HT), achieving the firing of action potentials in the neurons with high reproducibility [35]. Also, very promising results have been recently obtained with a P3HT-based substrate for skeletal muscle cells alignment and photostimulation [36]. However, the actual mechanism of photostimulation of such active substrates has to be further investigated and refined.

A significant number of diseases are associated with disfunctions of fundamental processes in electrochemical dynamics at the cell membrane, and the ability to stimulate cells selectively and efficiently can provide the opportunity to control, modify, and even heal damaged tissues. The above-mentioned techniques and studies have already evidenced this possibility, that could have a huge impact on human society. In particular, exogenous optical stimulation holds the potential to be the groundbreaking approach to excite cell activity and worthy efforts are being made in this direction. Importantly, a multidisciplinary common language is the crucial

point for such a field of research that requires refined knowledge of optics, biology, and material science.

Chapter 2

Perovskite: physics and optical properties

Generally, the term *perovskite* is referred to a kind of crystal structure with chemical formula ABX_3, where A and B are positive-charged ions and X is a negative-charged ion. This term was pronounced for the first time to entitle some particular cubic crystals in Russia that were named after a famous mineral collector, Perovskij [37]. These crystals were basically calcium titanate ($CaTiO_3$), but then the name perovskite was also applied to the class of compounds which have the same type of structure, called the perovskite structure. In origin perovskite were thought to be only metal oxides compounds with some ferroelectric and piezoelectric properties, that they do not exhibit suitable semiconducting properties for semiconductor applications. Later on, another class of perovskite, the metal halide perovskite, was discovered at the end of the 19th century [38], where oxide anions were replaced by halide ones. However, it was only from late 70s when large organic cations were used in the A position replacing metals that perovskites started generating interest in the field of Optics and Photonics [39] [40]. Indeed, this last type of perovskites, also called organic lead halide perovskites (CH_4PbX_3, $X = I, Br$), was found to be an excellent absorber for photovoltaic applications only in 2005-2006 in Japan [41], triggering a wide field of research of immense potential. One of that first organic inorganic structure, the methyl-ammonium lead iodide perovskite ($CH_3NH_3PbI_3$ or $MAPbI_3$), namely MAPI, was chosen as the starting point material of this study, given its outstanding optical properties and, more importantly, being probably the most investigated (and therefore consolidated) structure in literature. In this chapter, some of the most important features of organic inorganic perovskites are briefly discussed, with a particular focus on MAPI.

2.1 Material structure and optical properties

Despite the early discovery, the physical structure of halide perovskites has been explored only recently and not everything has been set yet. the first thing to say is that, unlike their more famous old brothers, like Si or $GaAs$, they are not composed by covalent bonds, but they belong to the class of ionic crystals, still exhibiting semiconducting properties. The typical crystalline structure is shown in Figure 2.1.

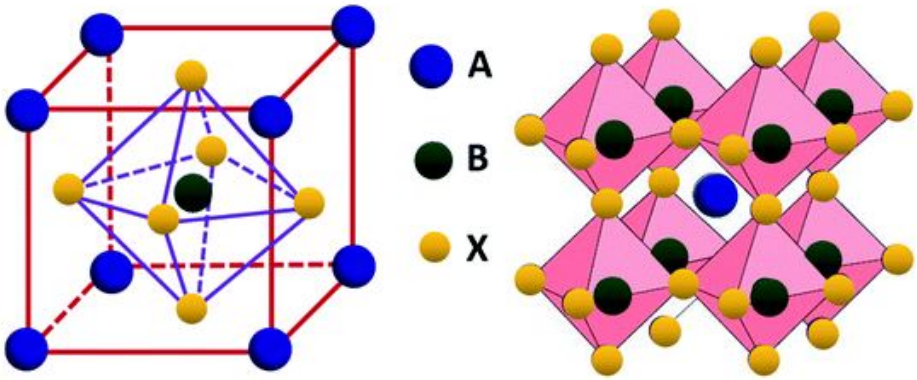

Figure 2.1. Structural arrangement of a typical perovskite crystal. Taken from [4].

Starting from the formula ABX_3, the B and X ions form the BX_6 octahedra with B in the center and X in the corner. Then, by connecting the corners, the BX6 octahedra extend to form a three-dimensional structure [42]. Three are basically the factors which influence perovskite formation: (1) the neutralization of charge between anions and cations, (2) the stability of the BX_6 octahedron, and (3) the ionic radii of A, B and X, that have to meet particular requirements so that the crystalline arrangement could be stable. If the first of the three can be trivial, the other two are critical in the perovskite structure formation. The octahedron stability is predicted by the ratio of the B-cation radius (r_B) and the halide counter ion (r_X), which is also called octahedral factor (μ), and, for values of μ between 0.442 and 0.895, it is shown to be thermally stable. The third requirement, instead, is described by the Goldschmidt tolerance factor t, which is the most important parameter to evaluate the presence of a perovskite structure. It is calculated by the formula:

$$t = \frac{(r_A + r_X)}{\sqrt{2}(r_B + r_X)} \tag{2.1}$$

where all the ionic radii are involved. Empirically, a perovskite crystal is found to be at $0.8 < t < 1.0$. Briefly, a coefficient between 0.9 and 1.0 indicates the formation of the ABX_3-type perovskite having the typical cubic unit cell, with the ideality reached for $t = 1$, whereas in the case of a t between 0.80 and 0.89, a distorted perovskite structure is most likely to be formed. For t smaller than 0.8, the A-site cation is too small to form a perovskite and, on the other side, t greater than 1 means that the A cation results to be too large. In this terms, MAPI is formed by a large organic cation in the A-site, the $CH_3NH_3^+$ (MA), closed by the octahedron composed by Pb^{2+} and I^- anions. Given their effective ionic radii, this brings to an ideal tolerance factor very near to 1 (0.912) and a octahedral factor of 0.541, making it a very reliable archetype of perovskite structure.
Among other halide perovskites, MAPI, which is a standard perovskite absorber in photovoltaics, possesses excellent optical properties useful for visible light optoelectronic applications. It can be classified as an intrinsic semiconductor with direct bandgap, exhibiting remarkable mobility of both photogenerated electrons and holes. The valence band (VB) of MAPI consists of approximately 70% of I $5p$ orbitals and

25% of $Pb\ 6s^2$ orbitals, while the conduction band (CB) consists of a mixture of Pb $6p$ and other orbitals [4]. The exceptionally high optical absorption coefficients of this material ($10^5\ cm^{-1}$) is owned to the direct band gap originated by the high symmetry of the unit cell and $p-p$ electronic transitions from VB to CB. Moreover, MAPI possesses a unique defect tolerance, due to the fact that the conduction band minimum (CBM) is very close to the Pb p orbital, as well as the valence band maximum (VBM) is close to the I p orbital. Therefore, vacancies formed by removal of I^- or Pb^{2+}, generate defect or trap states that reside respectively within or very close to the VB or CB, unlike other ionic semiconductors, where localized non-bonding orbitals surrounding the ion vacancies generally form trap states deep within the band gap, thus degrading carriers generation and transport. Therefore, since optical properties of MAPI, like other perovskites, is not significantly affected by eventual defects or vacancies, it is said that perovskites have a defect-tolerant nature. This, together with the exceptional absorbing properties, leads to large carrier diffusion lengths and long carrier lifetimes, that correspond to remarkable open circuit potentials (V_{OC}) and photo-conversion efficiency. Moreover, MAPI has the so called *ambipolar carrier mobility*, exhibiting similar effective mass values for both electrons and holes (0.23 - 0.29) [43]. Thus, as in inorganic semiconductors such as Si and $GaAs$, photogenerated carriers in perovskites behave essentially as free carriers, migrating in the perovskite absorber layers and giving rise to the photovoltaic process, as explained in the next paragraph.

2.2 Perovskite-based solar cell: working principle

The working mechanisms of a perovskite-based solar cell (PSC) has been object of discussion for years and today it is widely accepted that the working principle of PSCs is very similar to those of n-i-p and p-i-n standard solar cells. Here, the perovskite material has the role of the intrinsic semiconductor (i) sandwiched between two selective contacts (p and n). Typical n-type electron transport materials (ETM) combined with perovskites are TiO_2 for the n-i-p structure, and PCBM (a fullerene derivative) for the inverted p-i-n structure. Then, regarding p-type or hole transport materials (HTM), the most common are spiro-OMeTAD (an organic molecule) for the n-i-p, and PEDOT:PSS (a polymer mixture of two ionomers) at the bottom of a p-i-n type PSC. This kind of structure typically lays on a conductive substrate made of a metal oxide like FTO or ITO and is closed with a metal contact in Au or Ag. The perovskite absorbs light to generate the photo-couple. Then, the electrons are selectively collected by the ETM layer, while the holes are collected by HTM layer. The conductive paths at the bottom and at the top of the cell serve as necessary elements to interface circuitry. Figure 2.2 shows the band diagram of a typical perovskite device (FTO/TiO2/perovskite/spiro-OMeTAD/Au). Although this working principle might seem simple and intuitive given a previous background in standard solar cells, the processes that characterize a PSC are not as straightforward as they are in the common Si p-i-n solar cells. The complexity of phenomena such as accumulation, carrier generation, separation, and transport due to the interdependence of numerous features like grain boundaries, compositional non-uniformity, and interfaces still need further investigation.

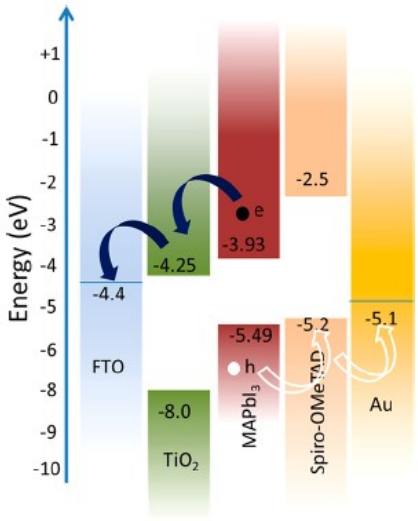

Figure 2.2. Energy diagram of a typical perovskite solar cell using $MAPbI_3$ as the perovskite absorber, TiO_2 as the ETM, and spiro-OMeTAD as the HTM. FTO and Au are the front and back contacts [4].

2.3 Stability concerns

It is nowadays common knowledge that the major concern about perovskite materials is their peculiar instability with respect to external agents. This is the greatest obstacle that prevents them from becoming the new frontier of photovoltaics, at the point that some studies doubted of its potential future in this sector [42]. Four are the principal factors that affect metal halide perovskites behaviour altering their intrinsic physics [44]: (i) moisture and, in general water; (ii) oxidation; (iii) photodegradation; (iv) thermal stress. Given this fragile behaviour, an appropriate packaging or passivation technique is required for applications involving perovskites, especially in physiological environments. Water, and therefore also moist environments, are surely the most troublesome enemy of the stability of a salt like a perovskite crystal. Water molecules are pervasive and make the crystals suffer from corrosion, pretty much like any other material of this kind. Specifically, H_2O molecules in the organic-inorganic perovskite form strong hydrogen bonds with the organic cation, weakening the bond between the cation and the PbI_6, thus allowing for faster deprotonation [45]. Unpackaged, exposed to air, MAPI samples are supposed to degrade completely in few days. This is certainly due to humidity, but also to the presence of oxygen. Oxidation not only affects the active absorber layer, but also the charge transport layer, especially if it is a polymeric compound. In fact, it is known that polymers are pretty susceptible to oxygen molecules. Any oxidation-induced defects can result in increasing recombination losses and damaging charge separation and collection from the perovskite layer, but do not affect the performance in terms of optical properties like carrier generation, making oxidation of polymeric charge transport layer not as crucial as the one of the absorber. Indeed, for some HTLs, like for example spiro-OMeTAD, a certain grade of oxidation is required to enhance their hole conductivity [46]. On the other hand, the perovskite active layer, although relatively tolerant to oxygen in dark conditions, is proven to be very fragile in presence of

the combination of oxygen and light, which is actually the most common operating condition, due to the arousal of reactions of photo-oxydation [47]. In practice, iodide vacancies mediate the photodecomposition process by leaving a path for oxygen molecules diffusion inside the crystal [48]. At that point, the adsorbed molecular oxygen effectively generate trap states in the conduction band of the photoexcited perovskite and easily form the superoxyde O_2^-, which is highly unstable and rapidily reacts with the acidic A-site cation (methyl ammonium in MAPI) leaving lead iodide and deprotonated gas. The reaction for MAPI crystals has been identified as follows:

$$4CH_3NH_3PbI_3^* + O_2^- \longrightarrow 4PbI_2 + 2I_2 + 2H_2O + 4CH_3NH_2 \tag{2.2}$$

In this sense, since iodide defects play a fundamental important role, controlling the density of these vacancies during fabrication would be crucial. If an ideal encapsulation of the device should prevent from undesired effects related to oxygen and water, the biggest issue would be represented by the intrinsic photostability, that is the actual tolerance of the material against illumination. In principle, encapsulated MAPI films were early on demonstrated to be resistant to light exposure of more than 1000 h with no sign of decomposition [49]. However, even if there is no sensible degradation of performances, many studies have proven that a number of purely photoinduced effects occur in the material, like increased ion migration, photo-segregation and also compositional changes [50] [51] [52]. Also the organic semiconductor (OSC) layers are not perfectly stable in the excited state and can produce free radicals which can undergo cross-linking, increasing the disorder in the polymer, though without extremely deleterious effects on the device performances [53]. Another concern about organic lead halide perovskites is how their stability scales with temperature. Indeed, thanks to their high tolerance factor 2.1 MA-based perovskites are structurally more stable than other similar counterparts like $FAPbI_3$ and $CsPbI_3$, but also suffer more from thermal decomposition. In fact, early studies using thermogravimetric analysis (TGA) have shown this multiple step reaction [54]:

$$MAPbI_{3(s)} \longrightarrow PbI_{2(s)} + [CH_3NH_3^+ + I^-] \longrightarrow PbI_{2(s)} + CH_3NH_{2(g)} + HI_{(g)} \tag{2.3}$$

Fortunately, none of these steps occurs at the operational range of temperatures (from -15°C up to 65°C), but this possibility must be taken into account in the fabrication stage 3.1, especially in the annealing phase. Here, the intention of driving away the excess of solvent at temperatures around 100°C has to be balanced with the possibility of decomposing the newly formed perovskite. It must be also mentioned that MAPI possesses two different photoactive phases with a transition temperature at roughly 55°C, between an high-temperature cubic phase (α) and the room temperature tetragonal phase (β), even if for the scope of this study the operational temperatures should never exceed the transition limit of temperature.
All the previous stability considerations have to be taken into account when dealing with the $MAPbI_3$ perovskite, which is the fundamental starting material of this study and has to be prepared to be resistant to air, water, light exposure and all other ambient agents. Many solutions have been proposed to address the poor stability of perovskite-based devices, by employing encapsulation materials and techniques for perovskite and organic solar cells according to the present understanding of reliability issues [55], but hardly anyone could fit the purposes of this study. In particular,

compared to photovoltaic applications, here perovskite films, whether they have to be interfaced with cells, shall comply with another essential requirement, which is biocompatibility. This is indeed a very tough task, given the toxicity of the material, especially due to the presence of heavy metal ions and its above-described intrinsic instability. Encapsulation can play an effective role in improving the stability of perovskite devices, acting as a barrier layer against the diffusion of oxygen and moisture (Figure 2.3). In general, the encapsulation layer should possess high light transmission,

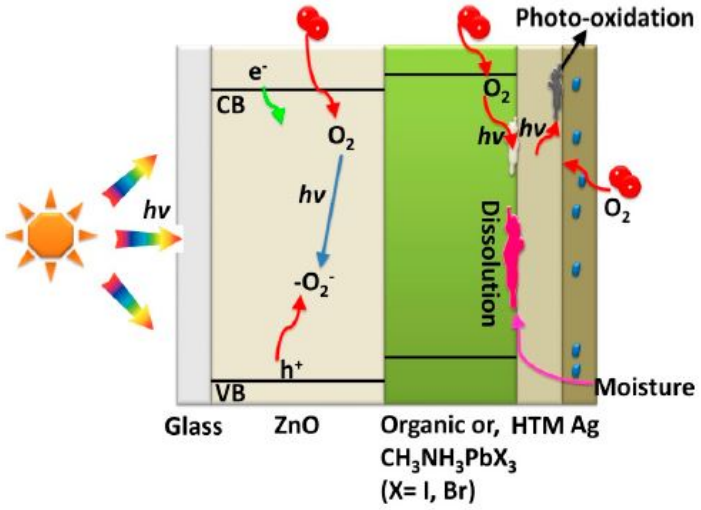

Figure 2.3. Electron-hole pair recombination, moisture dissolution of perovskite material and photo-oxidation processes at the interface between hole transport materials (HTM) and metal electrode are shown. Adapted from [5].

resistance to oxidation and thermal degradation, relatively high dielectric constant, and good process availability. These requirement have been translated in some key parameters displayed in table 2.1.

Table 2.1. Most important specifications for encapsulating materials for the protection of organic and perovskite devices from external agents. Data taken from [9].

Parameter	**Specification**
Total light transmission	>90% of incident light
Water absorption	<0.5 wt% at 20°C/100% RH
Oxygen transmission rate (OTR)	$10^{-3} - 10^{-5}\ cm^3\ m^{-2}\ day^{-1}\ atm^{-1}$
Water vapour transmission rate (WVTR)	$10^{-3} - 10^{-6}\ g\ m^{-2}\ day^{-1}$
Tensile strength	>3000 psi at 25°C

Uddin, Ashraf, et al. [55] reviewed the different encapsulation materials and techniques for perovskite and organic solar cells and possible obstacles to their applications. A wide range of silicon-based thin films [56], resins [57] and polymers [58] have been employed as shielding materials to increase devices lifetimes, each one with its own pluses and minuses according to the specific application, mostly directed toward photovoltaics.

In this study, a novel method of encapsulation was explored, based on the chemical vapor deposition (CVD) of a Parylene polymer conformal coating, as explained in section 3.2. Parylene is the commercial name for a specific family of highly crystalline polymers commonly used as film coating to protect sensitive devices and components from extraordinarily harsh environments. CVD technique does not require the use of solvents or curing agents and offers the possibility for an on-site growing of the polymer thin film, penetrating all the tiniest crevices that would be unreachable by other conformal coating techniques. Among Parylene families, Parylene C was particularly found to possess remarkable barrier properties that could be suitable for the specification limits listed peroviously. The table 2.2 collects some of the most important properties of this polymer. OTR (Oxygen Transmission Rate) and WVTR (Water Vapour Transmission Rate) of Parylene are much lower than the ones of other silicons, epoxy, or urethanes [55], evidencing a reasonable possibility for the use of it for the purposes of this study. In addition, Parylene is an FDA-approved material that is recognized as safe in terms of biocompatibility requirements (USP Class VI and ISO 10993) [59]. Also, dielectric properties of Parylene are remarkable, making it a very effective insulator, even at very thin thicknesses [60]. This has to be reminded when dealing with electrochemical characterization and the interpretation of results 4. Another beneficial point on the use of Parylene is that its outstanding protective properties seem to be quite thickness-independent [59] [60], opening for the possibility of very thin layers coatings for samples. However, it must be said that in this asymptotic regime of insulating and barrier properties, the encapsulation effectiveness is governed by the defects in the barrier layer [55]. Hence, the performance of single-layer, encapsulated devices is controlled by the nano-meter size structural defects typically generated from dust or the intrinsic or extrinsic roughness of surface, making the fabrication and passivation processes even more critical in terms of sample quality.

Table 2.2. A collection of the most relevant Parylene C physical properties in terms of encapsulation

Property	**Parylene C**
Insulation resistance	$3.2 \cdot 10^{10}$ Ω (0.0001*in* film thickness) [60]
Transmittance of light	>95% @$350 - 900nm$ (deduced from [61])
Water absorption	0.1 wt% [62]
Oxygen transmission rate (OTR)	2.8 $cm^3\ mm\ m^{-2}\ day^{-1}\ atm^{-1}$ [59]
Water vapour transmission rate (WVTR)	0.02 $g\ mm\ m^{-2}\ day^{-1}$ [63]
Tensile strength	10000 psi [59] [60]

2.4 Potential Applications

With their excellent optoelectronic properties perovskite-based materials can find potential applications in many fields, starting from photovoltaics to imaging and photonics. Recently, researchers at South Korea's Ulsan National Institute of Science

and Technology (UNIST) and the Swiss Federal Institute of Technology Lausanne (EPFL) have claimed a new record power conversion efficiency (PCE) of 25.6% in a single junction perovskite solar cell [64], which overhelmed the immediately preceding record of 25.2% by a KRICT/MIT group [65]. This achievement is even more impressive given that the conversion efficiency was only 3.8% in 2009 [66]. The rapid escalation of successive records in terms of PCE is a sign of the enormous interest that this kind of materials have generated in researchers of photovoltaic field, so that reaching silicon at 26.7% PCE seems an almost foregone conclusion now. Stability issues aside, there are concrete hopes that perovskite-based solar cells will be the first ever to reach the threshold of 30% PCE soon. Indeed, the new frontier of perovskite devices goes well beyond photovoltaic. Light emitting diodes (LEDs) are considered one of the most promising field of application, since perovskite-based LEDs have been proved to operate at very low driving voltage, giving superior advantage over the existing LED [67] [68] [69]. Conversely, staying on light-to-electric conversion devices, high responsivity photodetectors or light sensors based on MAPI perovskites have been successfully fabricated, with reported quantum yield that far exceeds 100% [70] [71]. Similarly, perovskite-based devices were found to be potentially suitable for imaging applications. *Yakunin, Sergii, et al.* have demonstrated that solution-grown single crystals of methylammonium lead halide perovskite can be used as pixels for full-color imaging [72]. Two years earlier, a similar technique that used a MAPI-based solution was employed to provide X-ray detection designed for real time medical diagnostic tools [73]. Moreover, *Wei, Wei, et al.* have shown that it is possible to integrate single crystals hybrid perovskites with well-established inexpensive silicon circuitry, significantly improving the performance of state-of-the-art X-ray imaging systems [74]. Perovskite have also been employed as energy harvesting modules [75] and power providers for wearable devices [76], giving promising results. However, notwithstanding the huge deal of research interest, perovskite are hardly thought as compatible with biological applications, given their vulnerability to water. Moreover, this demonstrates the innovativeness and the ambitiousness of this study. Nevertheless, some "inspiring" attempts to make nontoxic water-resistant perovskites and interface them with cells have been made. *Zhang, Haihua, et al.* demonstrated a strategy to overcome hydrolysis of inorganic perovskites by embedding $CsPbX_3$ ($X = Cl, Br, I$) nanocrystals (NC) into microemispheres of polystyrene matrix. This strategy was aimed at preparing perovskite NC multicolor luminescence probes in live cells. Using ten intensity levels and seven-color encapsulated NCs with non-overlapping spectra, they affirm that it would be possible to individually tag about ten million cells for biosensing and bioimaging purposes [77]. A similar approach has been also employed to embed $MAPbBr_3$ NCs, obtaining high photoluminescence efficiency, color purity, and ultrahigh stability against water exposure [78]. Furthermore, organohalide perovskites have already attracted pioneering attention for being an ideal candidate for photostimulation of neurons. *Aria, Mohammad M., et al.* claimed an high-level perovskite stability and biocompatibility by forming hydrophobic perovskite microcrystals and encapsulating them within a polydimethylsiloxane (PDMS) layer [79]. Indeed, their MAPI microcrystals were interfaced with P3HT to help dissociation of photogenerated carriers thus creating an high sensitive heterojunction that covers from the visible to the near-IR. In addition, the encapsulating layer of the biointerface was actually a mixture of P3HT and PDMS to improve the inherent conductivity of PDMS

alone. At the end, they were able to show that their perovskite-based biointerface did not exhibit any toxicity on cells, though presenting undesirable faradaic leakages of current. Continuing in the direction that has been traced by these interesting results, this study aims to pick up the thread of the matter and show that perovskites can effectively be used as a suitable interface for powerless and wireless photostimulation of cells.

Chapter 3

Materials and Methods

As anticipated in the introductory chapter, the final goal of this work is to study the interaction of the biotic-abiotic interface exploiting the phenomenal optical properties of perovskite materials, which are supposed to be good candidates to further explore the photostimulation processes once in contact with biological environments. In particular, as seen in the previous chapter, MAPI was selected among the other metal halide semiconductors, given its archetypal nature. In fact, the wide literature was useful to carefully analyze its features, both in terms of chemical structures and optical properties. However, due to the intrinsic fragile stability of this kind of materials, as previously explained in section 2.3, samples requires a careful and systematic preparation in order to avoid as much as possible any contact between MAPI's compounds and possible degrading agents, notably water, which is the main component of biological tissues and cellular environment. Furthermore, this procedure has to be wisely validated before that samples eventually interface the target of photostimulation and reach the last stage of the research. Given the novelty of this deployment for perovskites, samples were necessarily fabricated *ex-novo* and smartly customized to be ready for characterization experiments. In this chapter the various techniques are briefly displayed essentially following a temporal order in the logic flux of the experiments, starting from the sample fabrication procedure, moving to the characterization and the validation tests, closing with the electrochemical measurements.

3.1 Fabrication

In this study, optimizing the fabrication process was a a crucial milestone to be achieved, since reproducibility of samples had to be ensured to further proceed with the next steps of the project. For this reason, although the scope was not to obtain a particularly efficient device for photovoltaic applications, a systematic protocol based on photovoltaic cells manufacturing techniques has been followed, just to obtain a relevant quality in terms of optical properties that justifies the use of perovskites for photostimulation purposes.

3.1.1 Substrates treatment

The first step to move towards fabrication of thin films is the preparation of the substrate. Except for the test samples, for which standard microscope glasses were used, Indium-tin-oxide (ITO) coated glasses were treated for the subsequent spincoating. First, slides were cut with a diamond tip to obtain $25x25mm$ squares. Then, all the steps listed below were carefully followed:

1. Substrates were put in a becker and drawn into acetone.
2. An ultrasound sonicator was used for fifteen minutes for a proper cleaning.
3. Substrates were then put into an becker filled with ISO-propanol, just like in step 1.
4. Step 2. was repeated.
5. A nitrogen flushing was applied to avoid halos formation.
6. Just before spincoating, glasses were treated with UV-Ozone to increase their wettability.

3.1.2 Spincoating

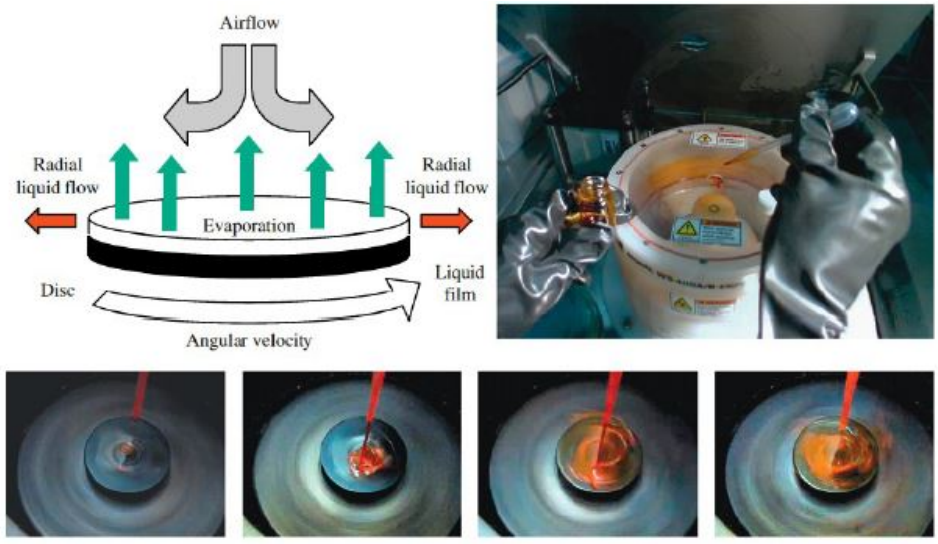

Figure 3.1. On the top left a schematic representation of the spincoating process. On the top right a real image of the spin coating operation. On the bottom a sequence of images that show the spreading of the solution. Adapted from [6].

Spincoating technique is one of the most common procedure of fabrication of thin films from materials that are dissolved in a precursor solution. The process is described in Figure 3.1: a drop of solution is deposited on the substrate kept on the sample holder by a vacuum pump; then, the instrument starts rotating at a fixed angular velocity, thus spreading evenly the content of the solution. At the end, the obtained film is homogeneous and its thickness is controlled by the rotation speed, the

time of rotation and the solution parameters. In this study, methylammonium lead iodide (MAPI) thin films were spincoated (at 4000 *rpm* for 30 *s*) using the so called *anti-solvent technique* [80], in a clean environment, starting from a precursor solution of lead(II) iodide and methylammonium iodide in dimethylformamide (DMF)/ dimethyl sulfoxide (DMSO) 0, 5 M. After spincoating, samples were left in a hot plate at 100°C for ten minutes. In addition, samples were also coated with an organic semiconductor (OSC), chosen between Spiro-OMeTAD (SPIRO) and Phenyl-C61-butyric acid methyl ester (PCBM). The first is one of the most suitable hole transport layer materials (HTL), whereas the second is often used in organic solar cells as an electron acceptor or electron transport layer material (ETL). The OSC coating was performed with the same instrument at 2000 *rpm* for 30 *s*. The thickness of both the MAPI and the OSC layers was also checked by means of a contact profilometer (Alpha-Step IQ from KLA Tencor). The spincoating parameters were adjusted to obtain a film thickness of approximately 150 *nm* for MAPI and 200 *nm* for the OSC layer. At the end, the final result was something similar to a typical solar cell, except for the fact that only one type of OSC layer was used at a time. The so-obtained samples were kept under clean environment, avoiding any contact with air, until they underwent the passivating treatment explained below. This was really important to ensure that the samples were not damaged by external agents.

3.2 Film passivation

As it was widely discussed in section 2.3, ensuring long-term stability of metal halide perovskite semiconductors is one of the most challenging task in the field of solar cells development and hence the great limit for effective applications of these materials. This is even more crucial in the goal of using these devices in contact with cells and their complex environment. In particular, since the materials in question are salts and take on water very easily, a uniform thin passivating layer sufficient to protect the perovskites from infiltration for more than 24 hours (minimum time needed for *in-vitro* experiments) is needed. In order to fulfill this severe requirement a Parylene conformal deposition was chosen as the winning solution. Parylene coating is already the ideal choice for a number of applications throughout the medical device and electronics and therefore was supposed to be a suitable choice also in this case. This process has a large number of advantages since it provides a systematic and high-value surface treatment with excellent moisture, chemical and dielectric barrier properties, by means of a ultra-thin, biocompatible polymer coating. The fact that the deposition takes place at the molecular level, where films essentially 'grow' a molecule at a time, is what makes this technique so outstanding in its functionalities. Parylene coatings are applied at ambient temperatures with specialized vacuum deposition equipment, as the one shown in Figure 3.2. The process can be summerized in these steps:

1. The raw material, in the form of dimer, is weighted with a precision balance so as to tune the resulting thickness.

2. Under vacuum, once the dimer is put into the chamber, the last one is turned on until the generated heat reduces the solid precursor into a dimeric gas.

3. The resulting gas is then pyrolized to break down the dimer to its monomeric form.

4. In the deposition chamber, where samples were previously placed, the monomer gas settles on the surfaces as a thin and transparent polymer film.

This technique allows to effortlessly penetrate also really tight areas thus providing a complete and uniform encapsulation of the samples. Of course cleanliness is a significant factor in terms of proper parylene adhesion to a substrate, so particular attention must be spent in this regard with the samples. Nevertheless, this type of deposition technique stands for its versatility and performance capabilities in terms of layer thickness and compactness.

Figure 3.2. A picture of the parylene coater setup.

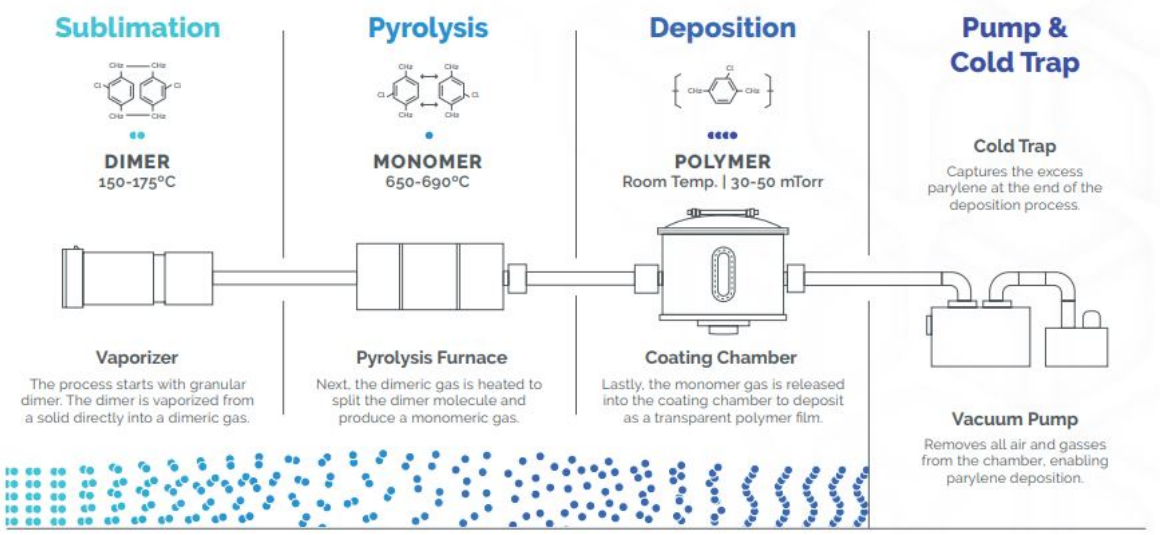

Figure 3.3. A detailed scheme of the procedure for parylene coating. Taken from VSi Parylene®.

3.3 Characterization

Once the manufacturing phase was finalized, the result was a glass/ITO substrate where a MAPI thin film and an optional OSC layer lay upon, all encapsulated by an insulating and water-resistant layer of polymer. This type of sample had to be validated at each crucial step of realization, especially evaluating the stability of the optical-responsive materials in response to ambient condition and, above all, presence of water. Therefore, a step of characterization was needed to reliably monitor the status of the 'photovoltaic' film, both in terms of crystalline structure and optical properties. For this reason, absorbance and XRD measurements were collected at each phase of validation, in particular before and after exposure of samples to air and water, and also after electrochemical experiments.

3.3.1 Absorbance spectrum

For this kind of characterization a spectrophotometer has been used. In particular the Lambda 1050 UV-Vis-NIR of PerkinElmer was available. This kind of instruments are composed by these principal elements: a tunable light source, a monochromator, a slit, a sample holder, and finally a detector with its auxiliary electronics. The incident light is filtered by the monochromator and impinges on the sample at a specific wavelenght, so that the collected light from the detector placed behind the sample holder is a direct measure of the transmittance of the sample at that wavelength, which can be easily converted in the absorbance quantitity. In this way, by repeating the acquisition for the whole interval of wavelengths of interest, one can reconstruct the absorbance spectrum of the sample.

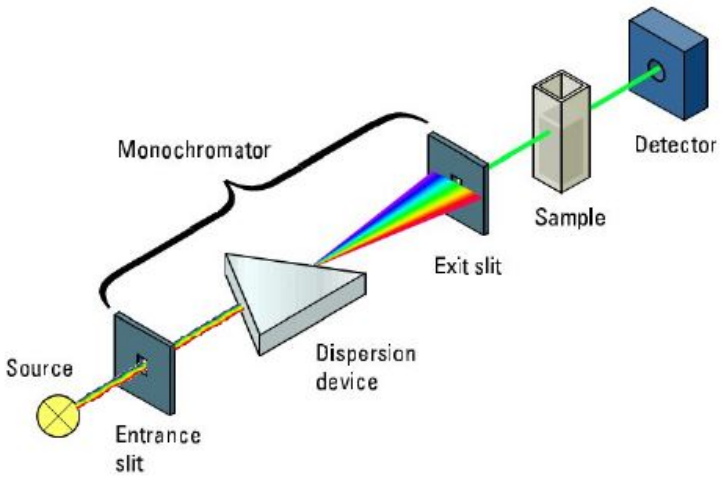

Figure 3.4. A schematic of the spectrophotometer setup. From left to right: light source, monochromator, sample and detector.

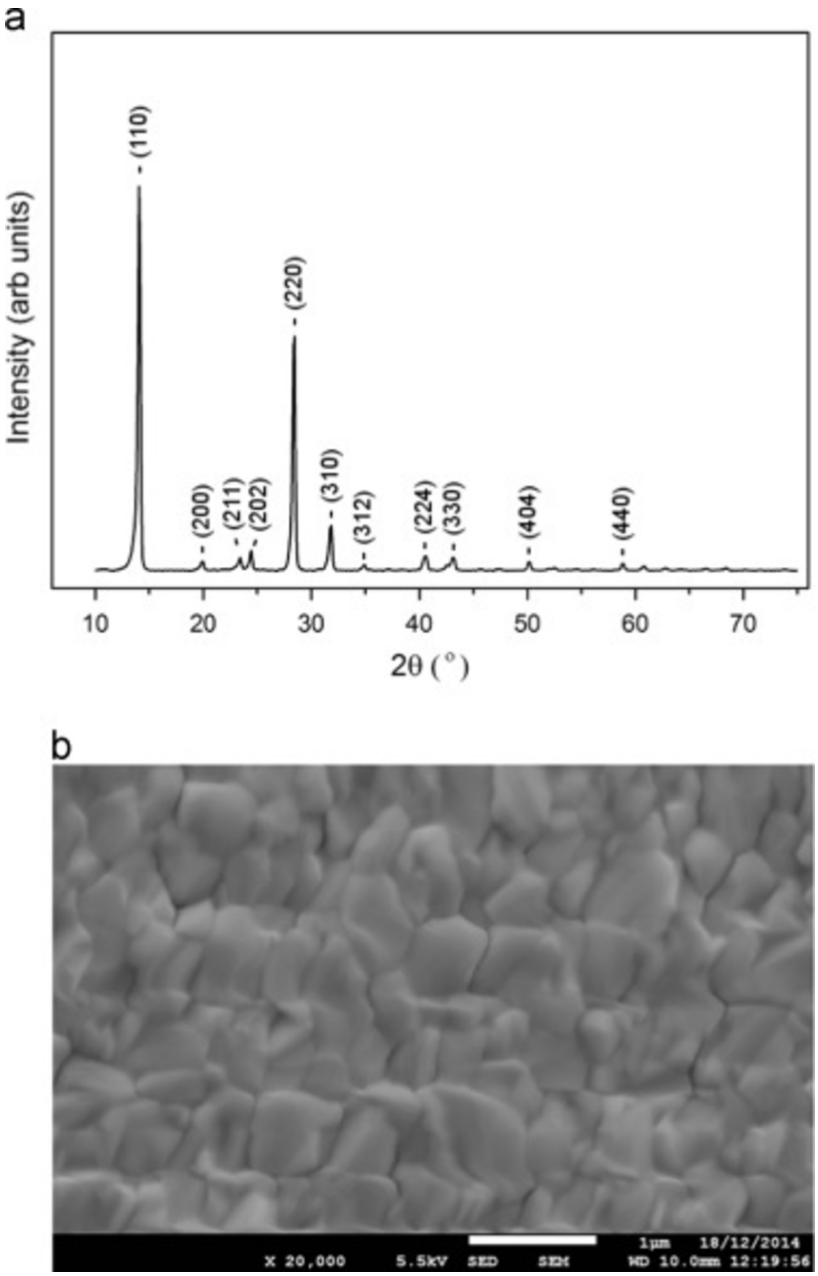

Figure 3.5. a) XRD data of a typical MAPI film; b) SEM image taken of the MAPI layer surface showing the grain structure and coverage. Taken from [7].

3.3.2 XRD measurements

X-ray diffraction (XRD) is a method for studying the structural, the compositional and the physical properties of both powders and bulk materials. XRD measurements are based on the phenomenon of diffraction. Diffraction occurs anytime a wave encounters an obstacle, but it assumes an important interpretation whenever the obstacle is composed by a regular array of scatterers, like it happens for crystalline matter. Atoms, ions or molecules in a crystalline matter, where they are arranged into regular arrays of repeating unit cells, act as secondary sources of spherical waves and scatter light in all directions when radiation hits them. Indeed, the so reflected waves cancel each other in a destructive interference phenomenon except when particular conditions are satisfied, only for a few specific directions. In those cases, the waves incur constructive interference and amplify each other generating typical bright spots of a diffraction pattern, identified by the Bragg Law 3.1:

$$2dsin\theta = n\lambda \tag{3.1}$$

where d is the distance between the diffracting planes, θ is the angle of the reflected radiation, n is an integer number indicating the diffraction order, and λ is the radiation wavelength. X-rays are used as appropriate electromagnetic radiation to produce the diffraction pattern since the wavelength of X-rays is more or less of the same order of magnitude as the atom distances in crystalline matter. When the samples are irradiated, X-rays primarily interact with the electrons in the atoms and scatter, producing the aforementioned diffraction pattern, which depends on the unique order of the atoms or molecules in every analyzed substance, according to the Bragg law. Inside the experimental apparatus, an X-ray analyzer measures the intensities and scattering angles of the X-rays diffracted from the material. The final result of the measurement is a plot having the X-ray intensity on the y-axis and the angle between the incident and the diffracted X-ray beam on the x-axis, which is conventionally called diffractogram. The presence of the diffracting planes is signaled in the diffractogram by the arousal of marked intensity peaks in correspondence of their specific angles in the x-axis. The XRD measurements of this study were taken by using a D8 ADVANCE-Bruker apparatus, focusing the attention on the characteristic peaks of perovskite structures, in particular the ones of MAPI crystals. As reported in Figure 3.5, the most evident peaks of the diffractogram for a MAPI thin film are placed at 14.1° (corresponding to the (110) principal plane), at 28.4° (corresponding to the (220) principal plane), and at 32.1° (corresponding to the (310) principal plane). Therefore, the XRD analysis was generally conducted between 10° and 30°, with a resolution of 0.1° at the incident angle of 1.5°. This kind of characterization is eventually extremely useful to monitor the crystalline integrity of the MAPI samples.

3.4 Electrochemistry

As anticipated, electrochemical characterization served as important tool to verify the behaviour of encapsulated perovskites in presence of wet environments, preceding the exposition to cells. These experiments have been conducted using potentiostatic and galvanostatic measurements and a three electrode electrochemical cell setup. The Metrohom PGSTAT302N equipment was used.

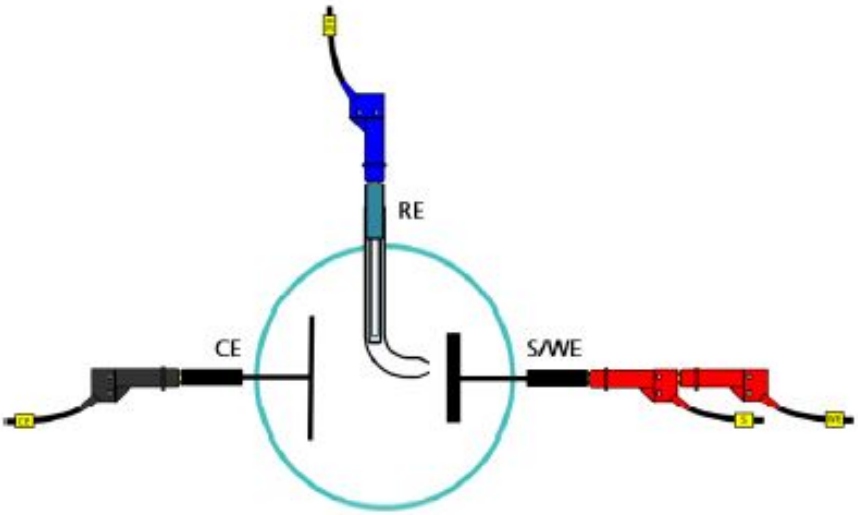

Figure 3.6. Schematic of the three electrode setup used in electrochemistry.

3.4.1 Working principles

In electrochemistry, potentiostatic/galvanostatic measurements require an electrochemical cell with three electrodes. Typically one has:

- The *counter electrode* (or *auxiliary electrode*) (CE), used to close the current circuit in the electrochemical cell. It is usually made of an inert material (e.g. Pt, Au, graphite, glassy carbon) so that it does not participate in any electrochemical reaction and simply acts as a source/sink of electrons.

- The *reference electrode* (RE), which has a stable and well-known electrode potential that serves as a point of reference in the electrochemical cell for the potential control and measurement. To guarantee this important feature, the reference electrode potential is usually stably defined by employing a reduction-oxidation reaction in which the concentrations of each participants are saturated. In essence, the requirements for a stable and non-polarizable reference electrode are an ideally null input capacitance and an infinite input impedance. This is approached by deviating all the current flow through the CE to close the current circuit in the cell together with a very high input impedance on the electronics of acquisition.

- The *working electrode* (WE), which is simply the electrode on which the reaction of interest is occurring and therefore the one against which the potential or current measurement is taken.

In potentiostatic mode, a potentiostat/galvanostat (PGSTAT) like the one employed will accurately control the potential of the counter electrode against the working electrode so that the potential difference between the WE and the RE is well defined. On the other hand, in galvanostatic mode, the current flow between the WE and the CE is controlled. Also, the potential difference between the RE and WE and the current flowing between the CE and WE are continuously monitored. All the experiments were conducted employing a the three-electrode cell setup. The three-electrode cell

setup is the most common electrochemical cell setup used in electrochemistry. In this configuration, the current flows between the CE and the WE. Meanwhile, the potential difference is controlled between the WE and the CE and so measured between the RE and the Sense electrode (S), which is indeed short circuited with the WE, like shown in the scheme in Figure 3.6. The potential between the WE and CE usually is not measured since it contains spurious potential drops given by the polarization of the CE and ohmic losses.

3.4.2 Custom setup

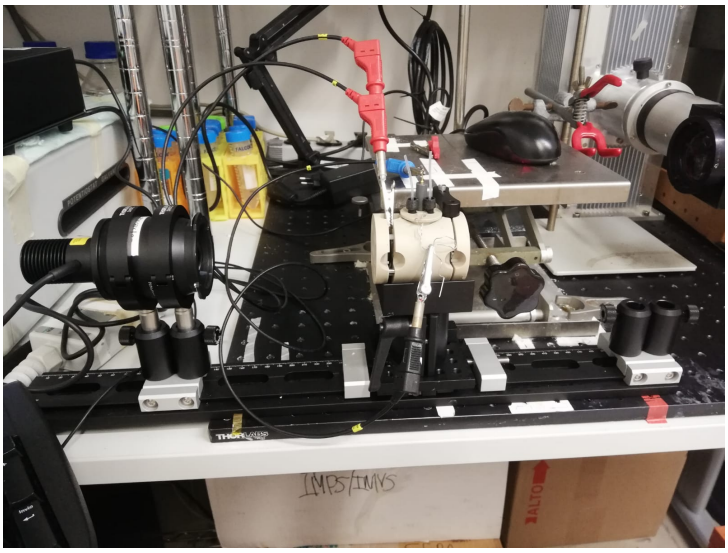

Figure 3.7. Picture of the electrochemistry setup used. On the left, the LED is connected to a digital driver and points to the electrochemical cell. On the right the electrochemical cell arranged in a three electrode setup ready for the experiments.

In the previous paragraph some fundamentals of a typical electrochemical cell setup were given, however the functionalities of an electrochemical cell are many and of different scopes. For this study, the idea was to observe the electrochemical behaviour of the perovskite samples when in contact with a saline solution and, at the same time, exposed with light. Therefore, the cell was arranged in a way that one side of the thin film could be exposed to a light of a LED and the other side, the one which was formerly encapsulated, could be interfaced with an electrolytic solution. One little edge of the samples was carefully cleaned with acetone to leave the space for an electrical contact with the ITO substrate, which was thus connected with WE through a crocodile clip. It is also important to say that during Parylene deposition, this edge was covered by a little tape so as to free the electric path with the ITO once the tape was removed. Then, a saturated $Ag/AgCl$ (Metrohm 60733100) was used as RE, while the counter electrode was a Pt wire (Metrohm 60301100). Both were drawn in the electrolytic solution and close the circuit as explained previously. A picture of the actual setup is shown in Figure 3.7. The solution was a 200 mM $NaCl$ solution in $Milli-Q$ water and not pH-adjusted. Also, a Pine Research RRPG147 quartz photoelectrochemical cell has been used. The light, instead, was supplied by

a green LED (Thorlabs M530L3-C5) working at 530 nm and driven by a DC2200 LED digital driver. The LED was placed at 25 cm from the sample and operated at maximum power, with a resulting intensity of light hitting the sample of 500 W/m^2. A very similar arrangement had already been used in a previous study to obtain a quantitative description of the fundamental mechanisms related to the photoactivation of P3HT [81].

Chapter 4

Results and Discussion

This study aims to demonstrate that perovskite-based substrates are good candidates to be suitable optoelectronic transducers for the photostimulation of cells. This chapter is dedicated to the presentation and the discussion of all the results collected towards this direction. An intuitive scheme of the final substrate after the manufacturing and the encapsulating stages is depicted in Figure 4.1. Over the glass/ITO slide lays the photoabsorbing layer of perovskite, which is in turn coated with the carrier extraction layer. The parylene polymer, instead, is the outermost layer and provides the insulating properties. The first essential point of the experimental activity was to demonstrate that the applied encapsulation technique is able to ensure a safe and stable interface with the living cells. The first part of the chapter is focused on that. Once the substrate's reliability was reasonably validated, the possible electronic response has been carefully analyzed through the electrochemical characterization. The last one is fundamental to have an idea of the electronic response of the substrate upon illumination and, therefore, to possibly predict the biological response when in contact with cells. The second part of the chapter presents these aspects. Eventually, the last part of the chapter is dedicated to the physical interpretation of the measurements. In particular, an equivalent circuit model was extrapolated from the physics of the system and adapted to experimental observations, giving interesting insights and interpretations about the substrate's behaviour.

Figure 4.1. Schematic of the sample substrate.

4.1 Insulating layer optimization

In the two previous chapters (chapt.2, chapt.3) the theoretical viability of the parylene CVD as a reliable method of encapsulation has been discussed. Depositing the polymer

at very low pressures should guarantee a non invasive, uniform and compact layer of protection for perovskite thin films against external agents. By lowering the deposition pressures, and therefore the deposition rate, the conformal nature of the parylene coating was exploited at its best. A deposition between 7 and 8 *mtorr* was employed for this purpose and layer of various thicknesses have been tested. In the experimental validation, the first point was to make sure that the polymer layer was not altering the underlying substrate. This was confirmed by XRD (Figure 4.2). It has to be noticed that the effect of parylene is to marginally enlarge the width of the characteristic peaks. This is particularly evident for the highest one at around 14.1° (110). This contribution is ascribed to X-ray scattering from the polymer layer which, as a result, gives a convoluted peak.

Then, the substrate was subjected to a series of stressing tests in order to effectively

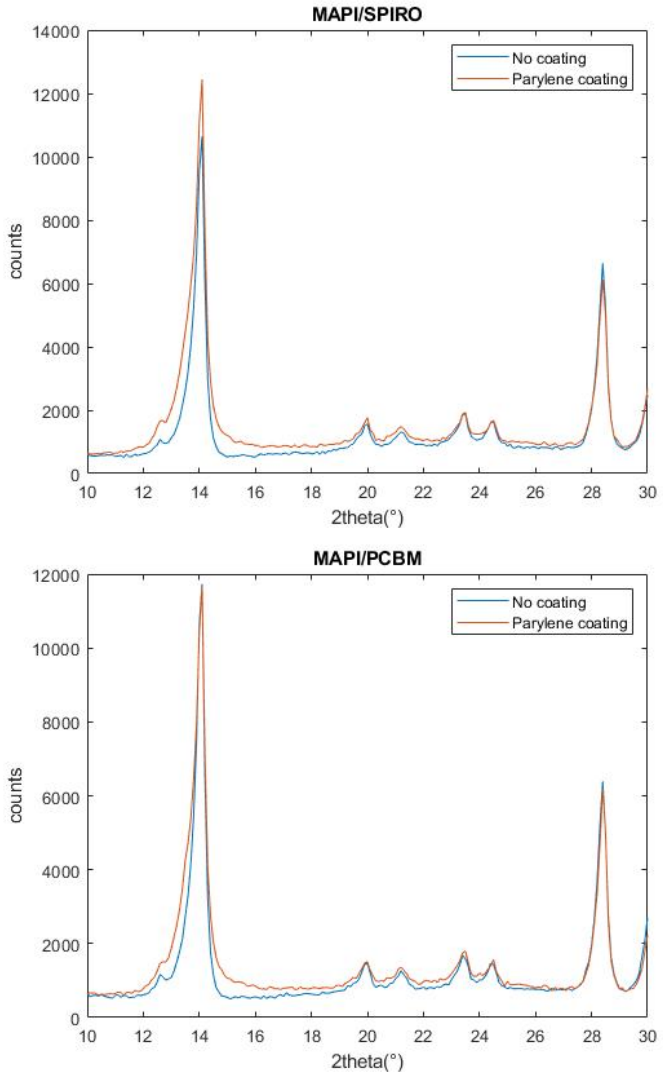

Figure 4.2. A comparison of the XRD diffractograms of the sample before and after the encapsulation with parylene. The characteristic peaks are slightly larger after the encapsulation, suggesting some spurious effects of the polymer structure in the scattering of X-ray light.

prove its stability in atmosphere and physiological environments. Specifically following

Figure 4.3. Couple of images taken during the water resistance test. On the left, a picture taken after samples been merged with water for an hour. On the right, the samples are shown after 4 hours of direct contact with water.

these steps:

1. exposure to air for 24 hours (previosluy stored in vacuum conditions);
2. thermal annealing (hot plate at 100°C for 2 hours) to simulate the sterilization step;
3. exposure to water for 4 hours.

The stability concerns of perovskites have been previously evaluated (see chapter 2), so that to prove a reliable encapsulation of the substrates against these agents will be a consistent success towards employment of perovskite for biological studies. XRD and absorbance spectrum measurements were taken before and after the treatments (Figure 4.4, Figure 4.5). The former verified the maintenance of the perovskite characteristic peaks, while absorbance measurement gave information on the preservation of perovskite optical properties. The results confirmed that the employed encapsulation is an effective way to prevent perovskites films from air, heat and aqueous environment for several hours. Yet, some of the samples still presented degradation after water contact. This is because the minimal defect in the parylene layer is responsible for irreversible infiltration. Moreover, the interesting tendency which has been noted is that the samples with an OSC layer were apparently more resistant than the ones with the MAPI layer only. This can be noted in Figure 4.3, where the sample 16, with the greater number of pinholes, is indeed without OSC coating. The reason for this observation can be due to both the further layer that separates the perovskite from the outside environment and to the fact that a better adhesion between the OSC structure and the Parylene molecule could be established.

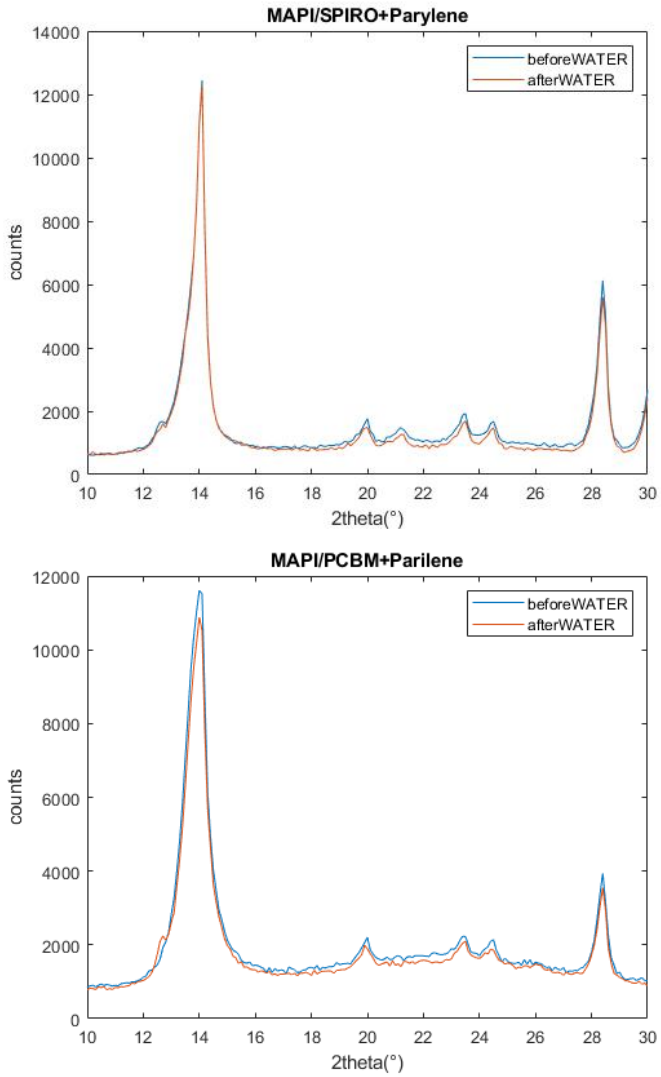

Figure 4.4. A comparison of the XRD diffractograms of the sample before and after the stressing tests applied. Thanks to the parylene encapsulation, a good conservation of the crystalline structure is observed.

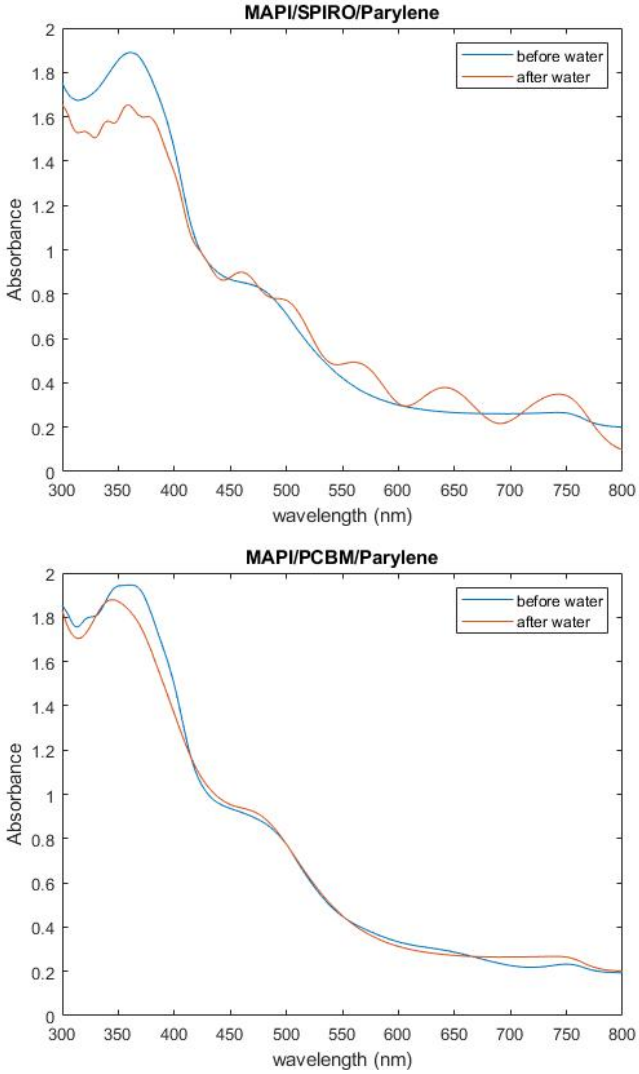

Figure 4.5. A comparison of the absorbance spectra of the sample before and after the stressing tests applied. The important absorbing property of the substrate seems to be preserved.

4.2 Electrochemistry measurements

The last step before approaching the phototransducing substrate to cells was an electrochemical characterization. With electrochemistry, in effect, one can model the interaction between the optoelectronic system and the electrolyte, giving insights for the possible behaviour once in contact with cells. This can be extremely useful to better understand the photo-induced processes that take place within the substrate and especially at the interface, playing a pivotal role in eliciting the biological response. The used setup has been previously described in chapter 3 (3.4.2). Three type of measurements were conducted:

- *photovoltage measurements*: it is a transient measure of how the resting potential of the substrate is varying upon illumination with the circuit left open. In this condition, the potential is commonly called *Open Circuit Potential* (OCP). The voltage measurement is taken between WE and RE, since the latter acts as a point of reference for potentials.

- *photocurrent measurements*: it is a transient measure of the amount of current passing through CE when the sample is exposed to light. For the purposes of this study, no external potential is applied to the system.

- *cyclic voltammetry*: it is another kind of potentiodynamic electrochemical measurements in which the WE potential is increased and then decreased linearly in cycles several times. The current versus the applied voltage is typically plotted to give a *voltammogram*. This test is useful to understand the behaviour of the substrate in the electrolyte upon the application of a potential, both in dark and light conditions.

It is important to keep in mind that for the equipment used, the maximum resolution possible for the transient measurements was 10^{-4} s.

4.2.1 Open Circuit Potential

The starting point of any electrochemical measurement is the potential measured when the system is electrically isolated and at rest. This value is commonly called open circuit potential. Before the system reached the OCP, a number of processes takes place, such as charge redistributions in the sample or in the electrolyte. Once a stable value for the OCP is set, the other measurements were conducted. The OCP values for the studied samples are quite variable among the set investigated. This is a matter of reproducibility, which is discussed in a specific section (4.4). Nevertheless, a coherence within each category of samples is present, giving the possibility for a statistical representation. These values are therefore reported in a box plot (Figure 4.6)

4.2.2 Photovoltage

Here after, the most significant photovoltage measurements are reported. The representative traces are taken by a transient measurement of the potential difference

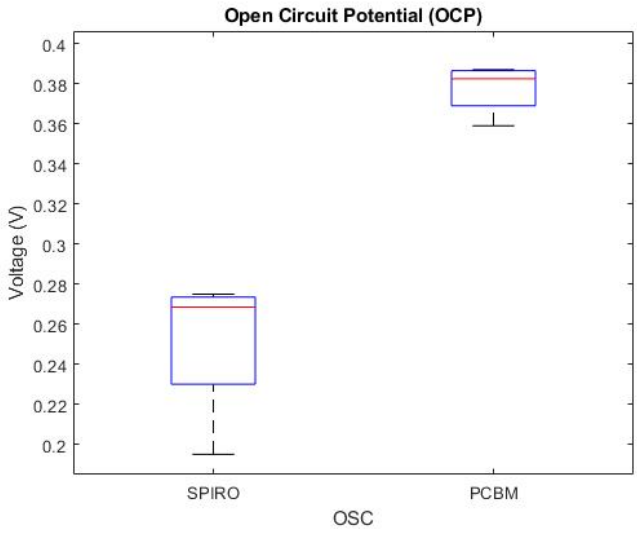

Figure 4.6. Box plot of the measured OCP values according to the different OSC. PCBM coated substrates have surely an higher value of OCP than SPIRO ones.

between WE (in contact with the ITO substrate) and RE (the $Ag/AgCl$ electrode immersed in the electrolyte). Data were acquired for 5 seconds, while a light pulse of 500 ms illuminated the ITO-side of the sample.
In essence, the traces show two types of sample's behaviour: (i) a very fast peaked trend given by electronic effects at the light on-off moments, and (ii) a much slower voltage shift due to a reaction of the system to the impinging light. It is important to say that the former can be resolution-limited, since the electronic time constants can likely be faster than the instrument resolution (10^{-4} s). For this reason, the amplitude of the peaks is probably higher than the one collected by the measurement. Moreover, light-on and light-off peaks are asymmetric both in sign and amplitude.
Importantly, these peaks are also of opposite sign according to the OSC layer present in the sample, as expected by the different charge carrier extracted. Theoretically, the slower trend is expected to have the same opposite sign difference between the HTL and the ETL. Yet, controversial results were collected (see section 4.4). Indeed, not all the samples confirmed this last aspect, suggesting that a further charged species is affecting the measurement. Reasonably, an ion species related with crystal defects and thus strictly connected to the fabrication process. It must also be reported that once the light stimulus is turned off, the system reaches the equilibrium with a characteristic time that ranges from tens of seconds to several minutes. This last behaviour, also called *self-healing*, is typical for perovskites, and has been deeply investigated in literature [8]. The authors attribute this asymmetry in the rise and decay of the photovoltage profile to ion migrations in the perovskite crystal (Figure 4.7). The ion charges redistribution induced by the charge carrier separation during illumination slows down the recovery of the system, due to its slower time constant (ions have lower mobility than electrons). Notably, the ion barrier acts as a charged shield against electron/hole back recombination.

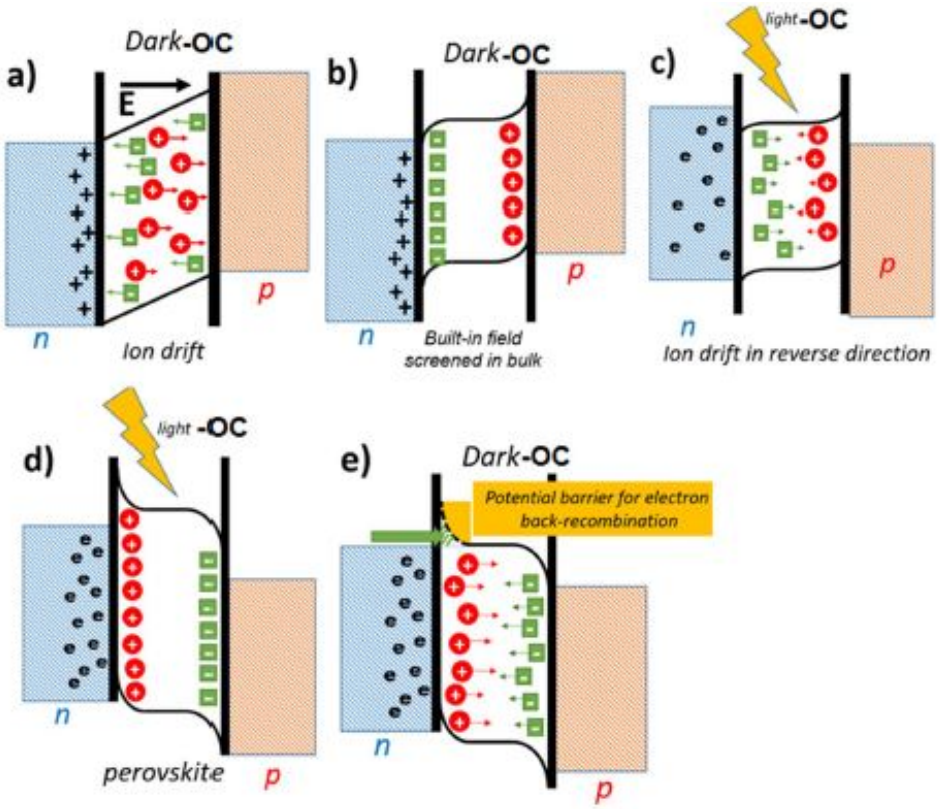

Figure 4.7. The energy diagram in perovskite absorber layer (a) Just after contact in dark, (b) in equilibrium in dark, (c) Just after light illumination, (d) in equilibrium under light, (e) after light soaking in dark. Taken from [8]. The physics of the self-healing process of MAPI perovskites is therefore explained by the influence of ion migration on the band diagram.

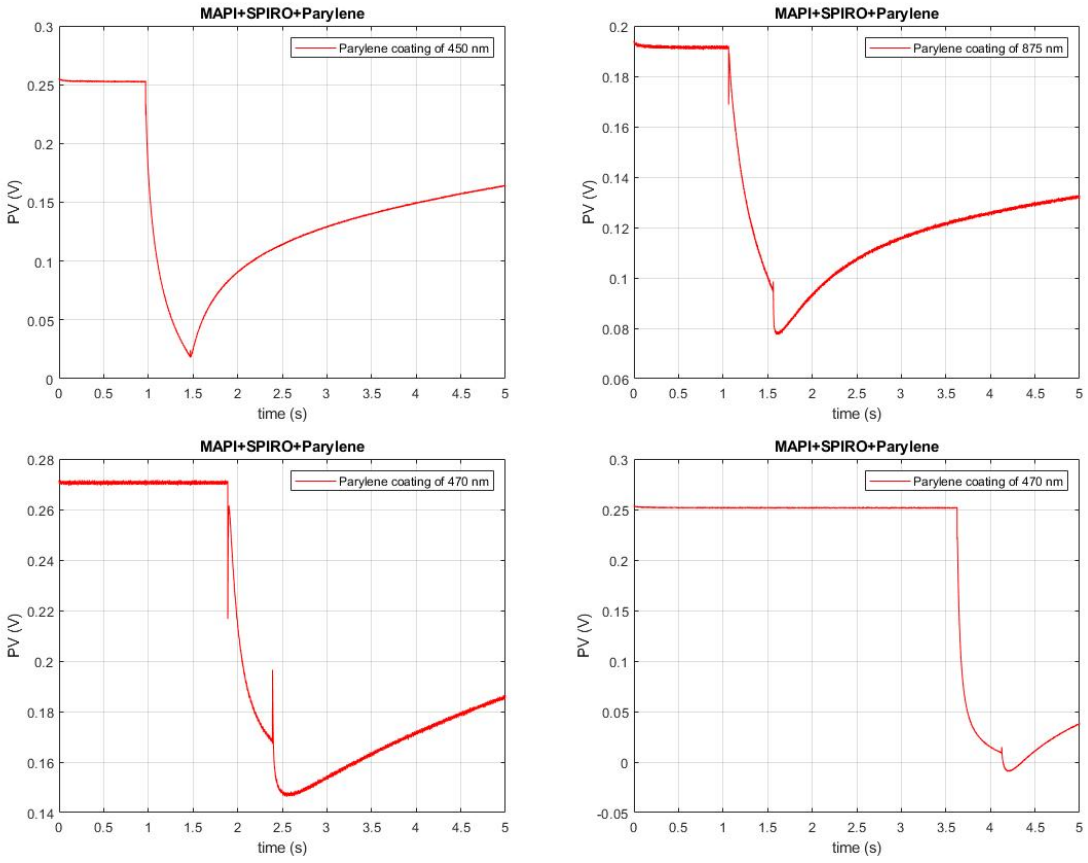

Figure 4.8. Representative traces of photovoltage measurements of four substrates with SPIRO that acts as hole transport layer. The ON-OFF peaks can be observed as well as the slower potential drop during illumination. When the LED is switched off, the self-healing process starts bringing the photovoltage back to the OCP.

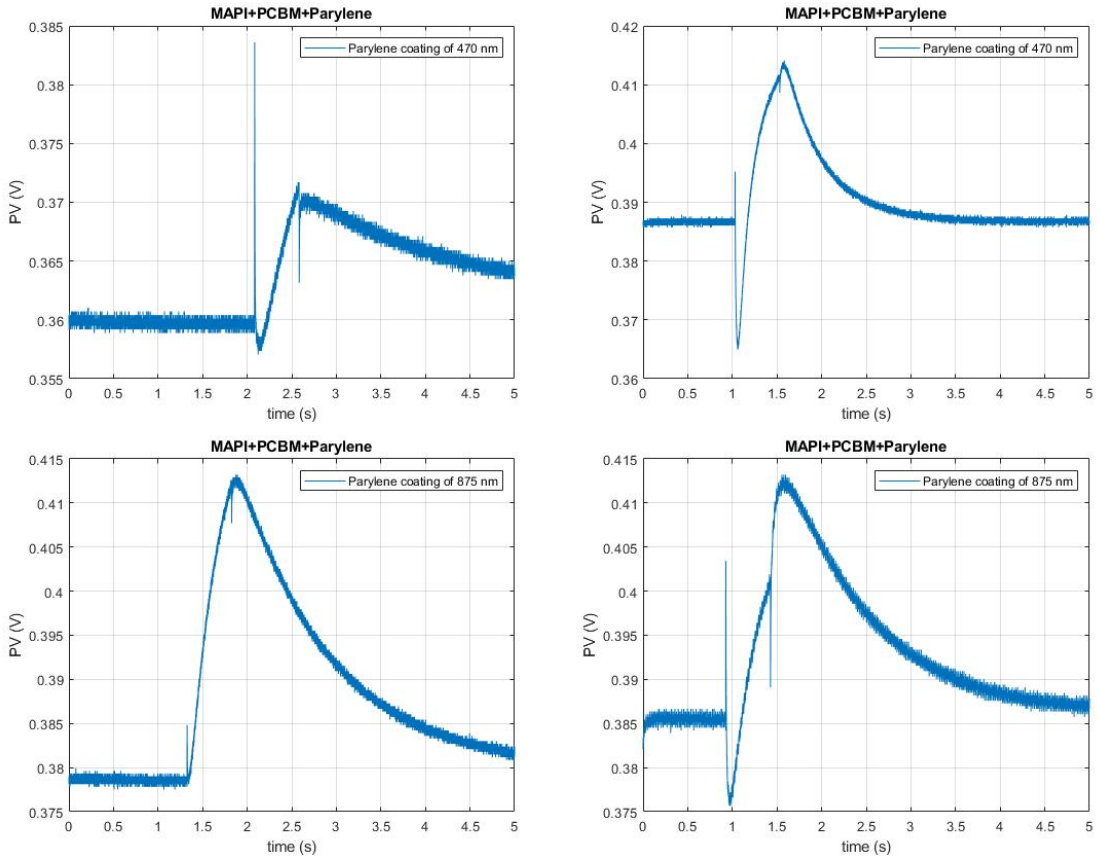

Figure 4.9. Representative traces of photovoltage measurements of four substrates with PCBM that acts as electron transport layer. Compared with the SPIRO-based substrates, the ON-OFF peaks have opposite sign. Also, the photovoltage slightly increases during illumination (contrary to SPIRO samples). Similarly, the self-healing process occurs at the switching of the LED.

Data Analysis

In the post-processing work, the time characteristics of the two most visible trends were extrapolated by means of an exponential fitting. For this purpose, a custom MATLAB code has been used. It is worth noticing that the fast electronic displacement was beyond the resolution limit of the instrument and thus it was not possible to investigate this aspect. Also, the self-healing process was not explored since outside of the scopes of this study. Only photovoltage curves were processed since photocurrent peaks were just tightly within the resolution of the instrument. Interestingly, a two-

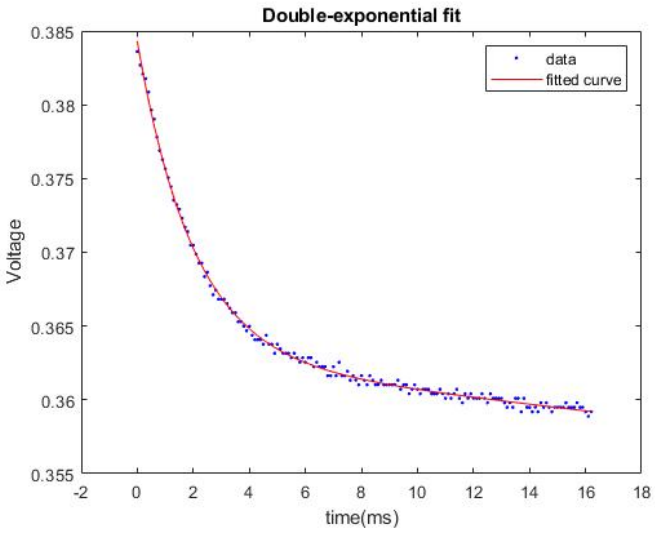

Figure 4.10. An example of how a two-exponential function is able to fit the peak decay of a PCBM-based substrate by using the proper MATLAB algorithm. The same accurate fitting was achieved for all the other curves analyzed.

exponential curve fitting was necessary to properly describe both the peaked decay and the slower voltage step. This can be a proof of the fact that two different charged species, correlated to each other, are affecting the response of the system. The values of the extrapolated time constants are reported in the Table 4.1. Although statistics should be reinforced with some other data, at least the order of magnitude of the temporal behaviour can be extracted. These values suggests the distinction between a fast electronic reaction to the stimulus, overlapped by a slower one, probably due to ionic species. Migration of ionic species mediated by vacancies in the perovskite crystal are in fact well documented [82] [52], although almost never studied in transient experiments. Moreover, a deeper focus on the amplitudes involved in the exponential fitting curves (see Figure 4.11 for a representative example) tells that the potential ionic influence on the voltage response can be remarkable, and surely dominant at longer time scales. However, this ionic-induced effect is difficult to control since it is most likely due to grain defects in the perovskite.

Table 4.1. The table collects the average values of the time constants of the fitted curves with their standard deviation. Data were extracted from 4 SPIRO and 4 PCBM-based substrates. The first column refers to peak rise/decay of the illumination peak. The peak was rising for SPIRO and decaying for PCBM. The second column, instead, refers to the photovoltage behaviour right after the peak, during illumination. In this case, the behaviour was opposite to the one of the peaks. The two time constants for each curve points out the presence of two distinct dynamic responses of the system to light excitation. Notably, during illumination, a behaviour that scales with a time of few seconds is identified.

	Rise/Decay of the peak	**Rise/decay during illumination**
SPIRO	$\tau_1 = 1.3 \pm 1.7\,ms$ $\tau_2 = 232.3 \pm 182.9\,ms$	$T_1 = 76.8 \pm 51.7\,ms$ $T_2 = 3.1 \pm 5.2\,s$
PCBM	$\tau_1 = 1.8 \pm 0.8\,ms$ $\tau_2 = 1.0 \pm 0.6\,s$	$T_1 = 331.5 \pm 225.8\,ms$ $T_2 = 19.9 \pm 14.0\,s$

```
General model Exp2:
f(x) = a*exp(b*x) + c*exp(d*x)
Coefficients (with 95% confidence bounds):
  a =      0.0634  (0.06322, 0.06358)
  b =    -0.02996  (-0.03014, -0.02978)
  c =      0.1704  (0.1702, 0.1706)
  d =   -0.004176  (-0.004181, -0.004172)
```

Figure 4.11. The post-processing output of the photovoltage curve of a SPIRO-based substrate. A much greater amplitude is found for the slower exponential behaviour. This distinction was present in all the analyzed samples, suggesting that the slower component of the signal (likely due to ionic rearrangement) is the dominant one at long time scales.

4.2.3 Photocurrent

Photocurrent measurements were conducted in the same condition as photovoltage acquisitions. In the following, the representative traces that correspond to the same samples of the previously displayed photovoltages are reported (Figure 4.12, Figure 4.13). As for the photovoltage curves, a peaked on-off behaviour is distinguished from a slower trend experienced during illumination. Here, the measurable effects during illumination are at least a third compared with the peaks of current immediately after the LED switches, not counting the possible data loss due to limited resolution. This suggests a 'capacitive' behaviour of the system in terms of current. In particular, the steady state photocurrent has been mostly cut down by the insulating layer of parylene, independently of the layer thickness. This last observation was expected, since parylene resistivity is very high and not so much influenced by its thickness. The other important thing to state is that, as for the photovoltage, the different signs of the on-off peaks according to OSC involved are a clear indication of the different carrier involved in the extraction of charges. Again, the amplitude values of the peaks could be higher than the ones measured due to the limited time resolution.

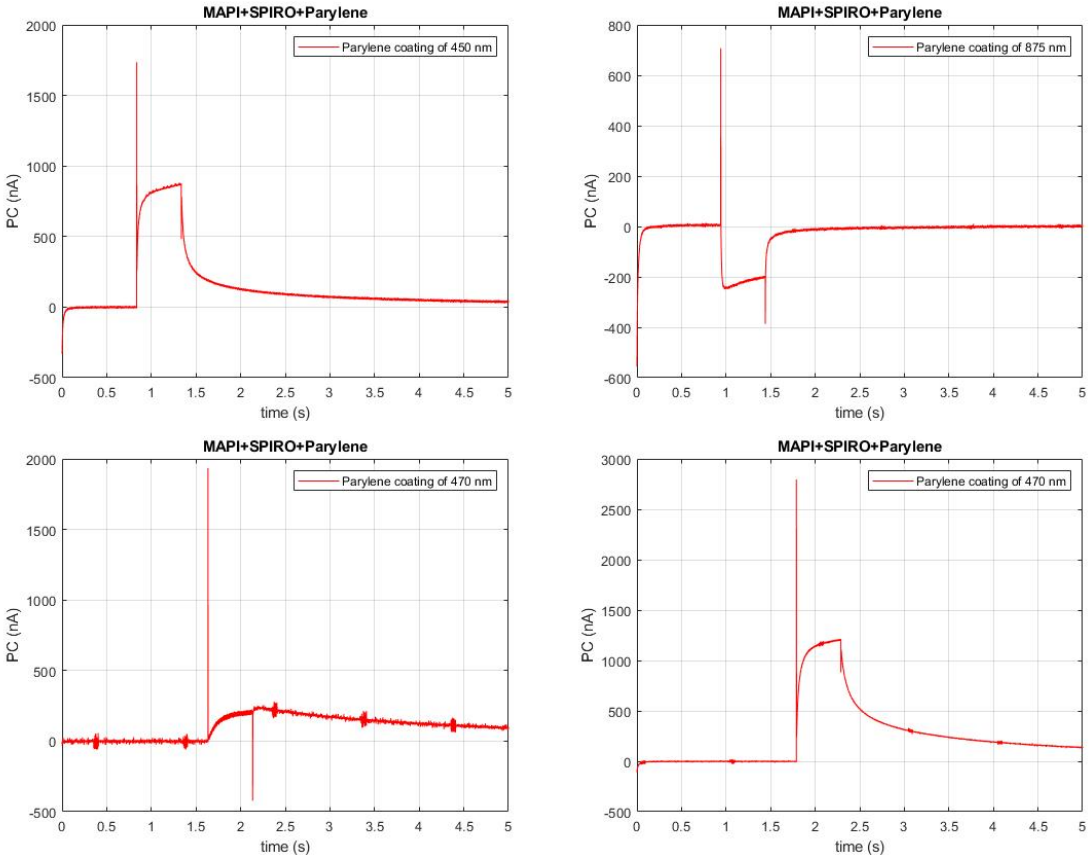

Figure 4.12. Representative traces of photocurrent measurements of the same four SPIRO substrates previously analyzed for the photovoltage. The ON-OFF peaks can be observed even if are just within the resolution limit of the instrument. A pronounced asymmetry both in sign and amplitude is observed.

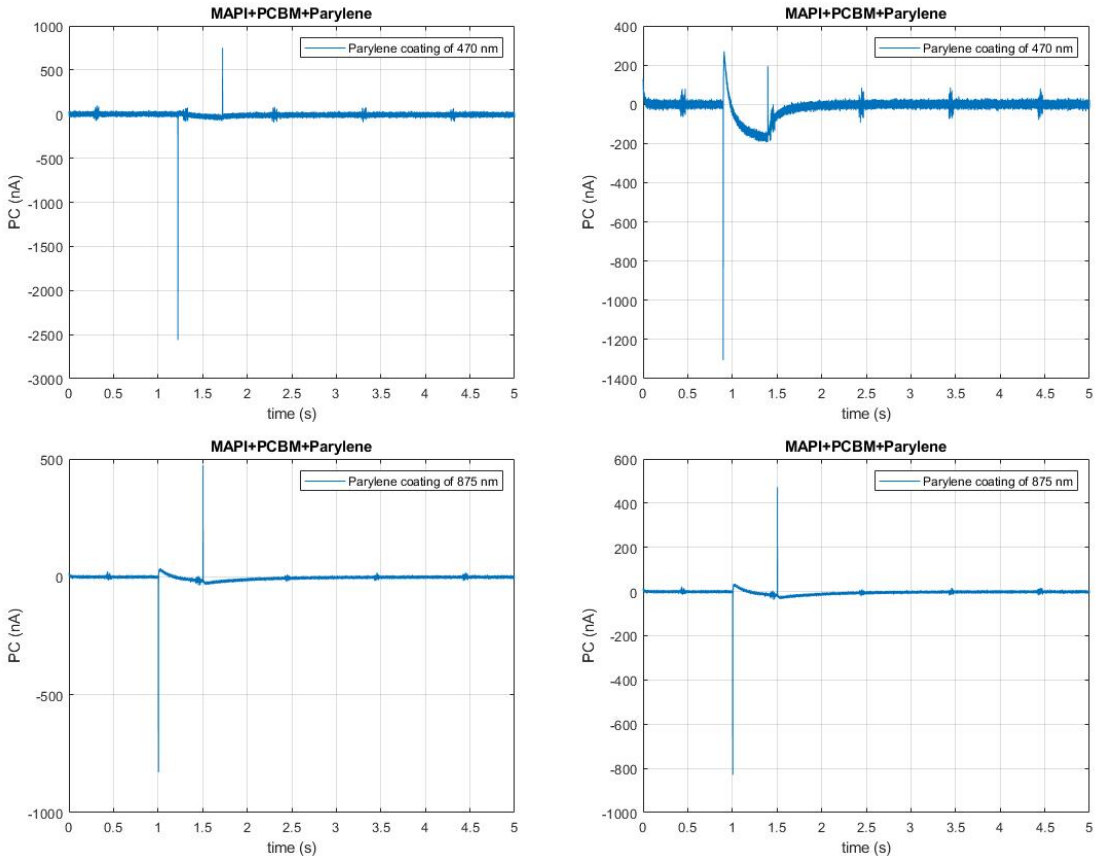

Figure 4.13. Representative traces of photocurrent measurements of the same four PCBM substrates previously analyzed for the photovoltage. The ON-OFF peaks are of opposite sign with respect to SPIRO. Here, the current during illumination is lower than the one observed in samples with SPIRO.

4.2.4 Cyclic Voltammetry

Cyclic voltammetry (CV) measurements were carried out for several samples of different nature (SPIRO coated, PCBM coated, no coating) in two different conditions: in dark and upon constant illumination. For the latter, sample was exposed to light for the time needed to reach the electrochemical equilibrium in light before performing the CV.
The results clearly indicate that in the condition of light exposure the conductivity of the system is increased, as evidenced by the higher slope of the I-V curve. This is expected for the increasing number of free charges that photoexcitation generates. The substrate with SPIRO and with PCBM, as expected, have higher values of current than the only-MAPI one, due to the enhanced carrier extraction (Figure 4.14).

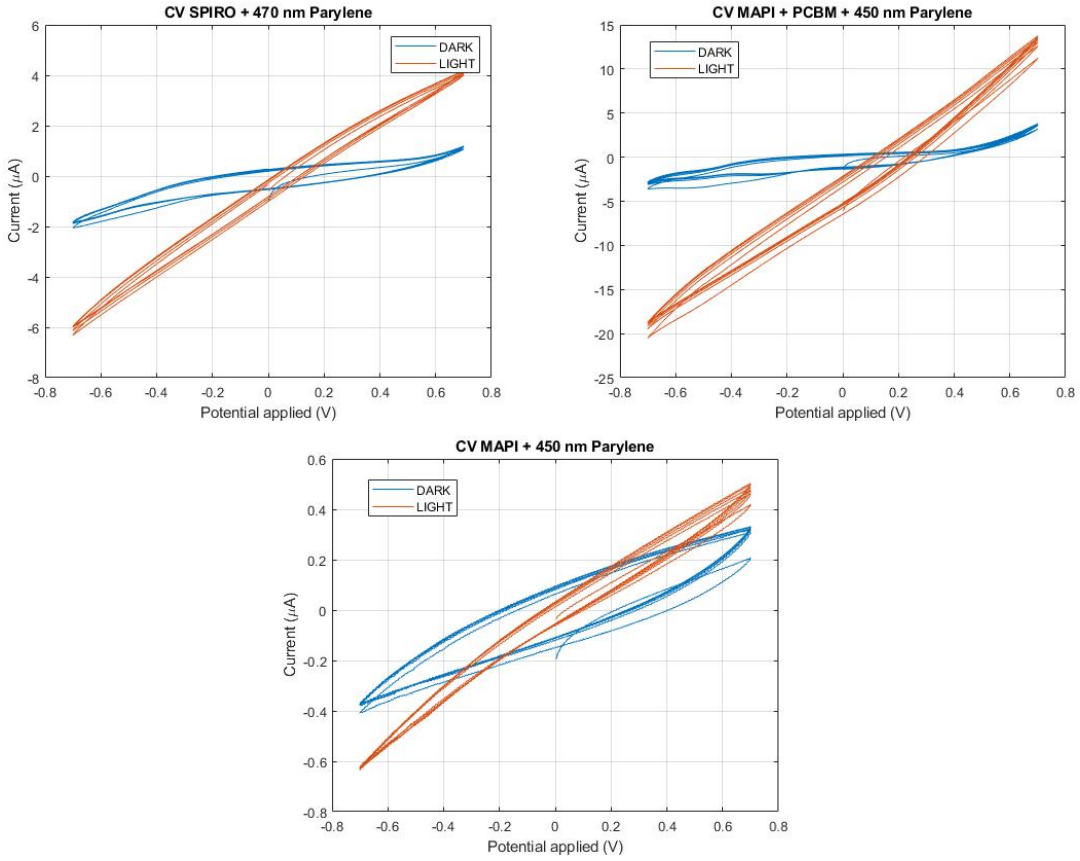

Figure 4.14. Cyclic voltammogram of the substrates both in dark and exposed to light. Both confirm a higher conductivity in light conditions due to the presence of photogenerated carriers.

4.3 Equivalent circuit model

4.3.1 The model

To better interpret the observed electrochemical behaviour of the system, an equivalent circuit model has been draft (Figure 4.15). In particular, the scope was to have a

reliable model of the response of the sample under light stimulation, discriminate the processes involved and identify the parameters that mostly affect the optoelectronic behaviour when interfaced with an electrolyte. To design the model (Figure 4.15),

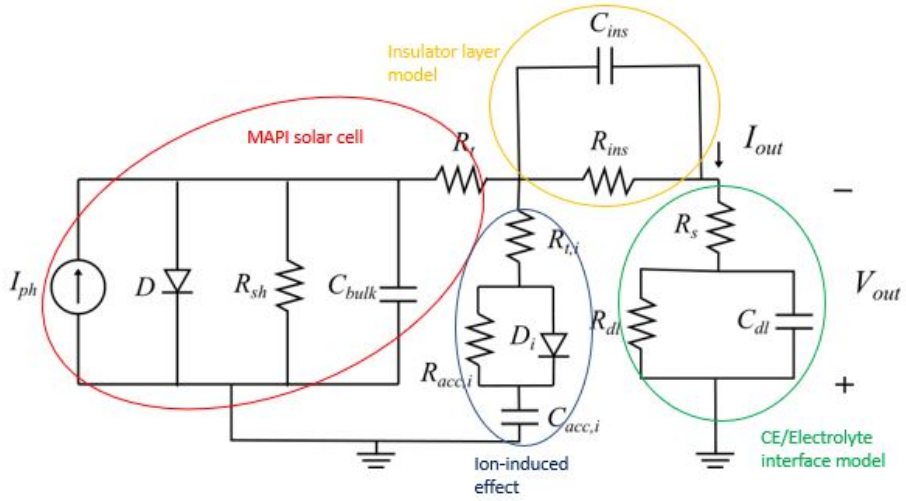

Figure 4.15. Schematic of the circuit model proposed.

already published equivalent circuits for specific parts of the system (both for the multilayer and interaction with the electrolyte) have been exploited. Ideally, the substrate composed by the glass with ITO, the perovskite thin film and its OSC layer can be modeled as a solar cell and its equivalent circuit. Beside the current generator that models the photogenerated carriers, the diode stands for the junction behaviour of the solar cell, R_{sh} represents all the ohmic losses of the cell, R_t the transport resistance, and C_{bulk} all the capacitive effects generated by the various interfaces between materials and contacts. This is a standard model for the solar cell equivalent and it is indicated in the scheme by a red line. The elements of the branch enclosed by the dark blue circle, instead, stands for the modelling of the self healing process. As described in the previous section (3.4), ions migrate in the crystal and can accumulate near the interfaces creating a sort of charged wall that forbids back recombination of electrons. This model has been previously validated in literature [8]. The $R_{t,i}$ stands for the ion transport, $R_{acc,i}$ models the highly resistive barrier for recombination, while D_i and $C_{acc,i}$ replicate the ion-induced junction generated by the polarization of charges, which caused the asymmetry in the relaxing time of the system. The insulating effect of the parylene layer passivating the whole structure is modeled by C_{ins} and R_{ins}, which, for the setup used, must be put in series since are directly in the electrical path of the circuit. Of course, the better the electrical insulation, the higher R_{ins}. Finally, the interface between the sample, the solution and the electrode that closes the circuit (CE) is modeled with a simplified version of the *Randles circuit* [83] (green-circled elements). R_s is a series resistance that models the conductivity of the solution and the electrode, while C_{dl} and R_{dl} stand respectively for capacitive and faradaic coupling of the electrode/electrolyte interface [84]. In particular, C_{dl} is the double-layer capacitance formed by the ion species in the electrolyte that gather near the electrode, while the resistance R_{dl} models possible charge transfers between the

solution and the electrode, which must involve redox reactions at the interface. This kind of model can be useful to the future understanding of the sample interaction with a cellular environment.

4.3.2 Simulations

In order to properly validate the model proposed, numerical simulations were conducted. LTspice has been used as analog electronic circuit simulator software. The circuit draft was imported in the software environment and a transient analysis has been performed to emulate the experiment conditions. Typical parameter values were taken from literature both for the perovskite-based solar cell [8] and the electrode/electrolyte interface [84]. The results of the simulation roughly replicate the main features of the experimental data. The capacitive peaks with their opposite signs are predicted, both for photovoltage and photocurrent, together with the steady state behaviour. As expected, the slow relaxation time is also well described by the model. Interestingly, the model gives information about the origin of the experimental measurements: the RC constant of the insulating layer of parylene is surely the major responsible for the capacitive behaviour of the system, since the insulator cuts down the steady state component of the signal. Then, the dynamic response of the solar cell is mainly affecting the amplitude and the width of the capacitive peaks. The slower behaviour of the signals, instead, is dominated by the coupling processes of the sample with the electrolyte, that is the Randles circuit's parameters.
By looking at the time scales, however, it is evident that the simulated data predicts narrower peaks for the photovoltage curve than the measured ones (hundreds of μs against a few ms). Indeed, the expected photovoltage on-off peaks are more or less of the same time scale of the photocurrent ones, whereas the measured photovoltage curves are at least one order of magnitude thicker. Furthermore, in the measurements the peak is typically followed by a sort of bouncing that brings the values of the photovoltage in the opposite direction. This is probably due to correlation between ionic and electronic effects in the system, that cannot be described by only independent generators or linear components in the circuit model. Eventually, it seems that the model fails to predict the slower component of the signal produced by the system, as if it lacks to describe the complicated interaction between ions and electrons that lives behind the perovskite substrate and its interaction with an electrolyte.

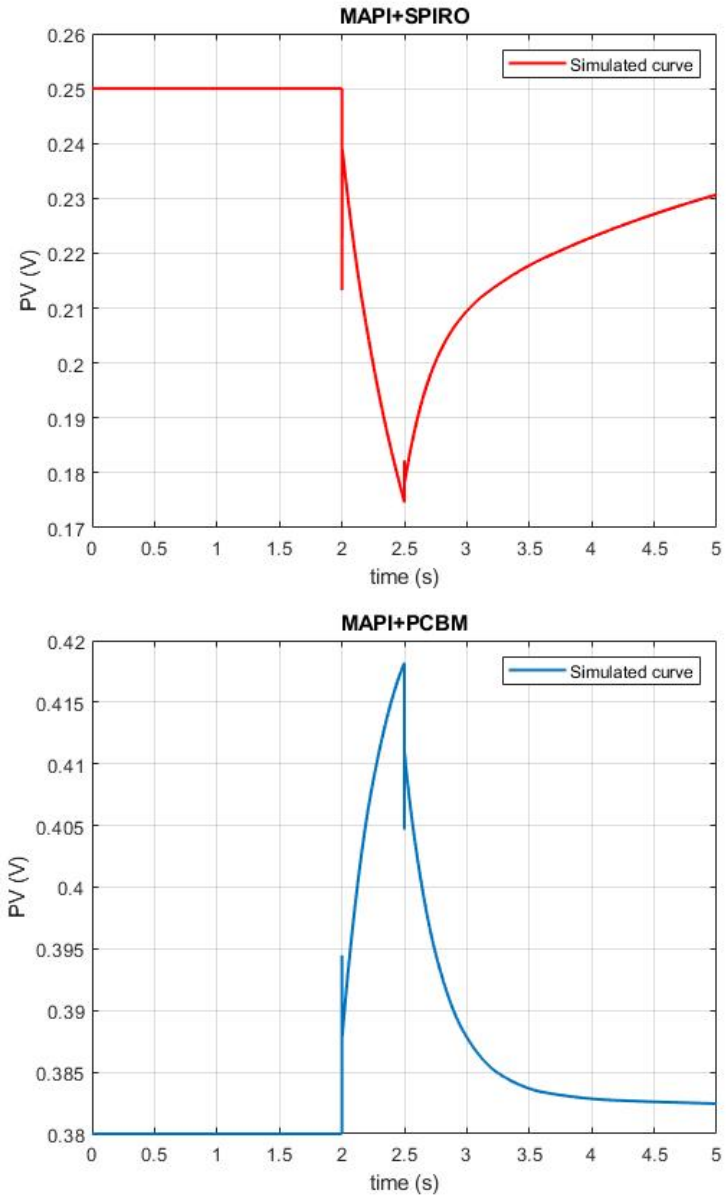

Figure 4.16. Expected profiles for photovoltage obtained from transient simulations. On the top, the simulated photovoltage curve of SPIRO-based substrates. On the bottom, the simulated curve of PCBM-based substrates.

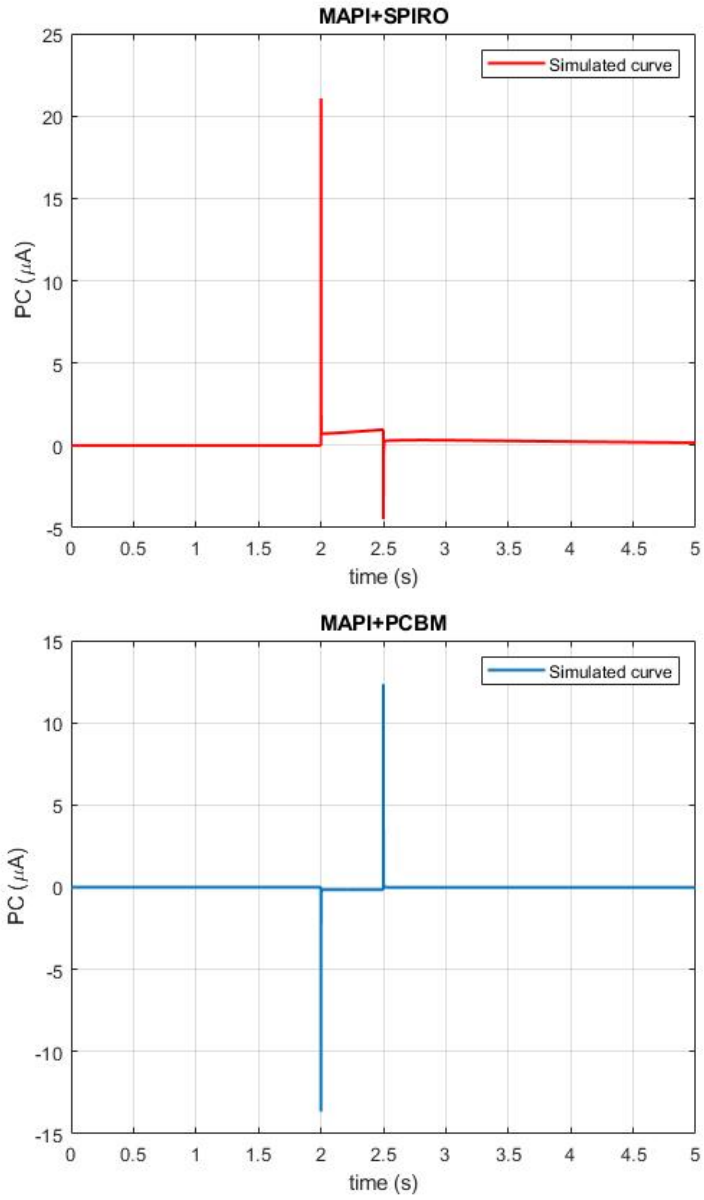

Figure 4.17. Expected profiles for photocurrent obtained from transient simulations. On the top, the simulated photocurrent curve of SPIRO-based substrates. On the bottom, the simulated curve of PCBM-based substrates.

4.4 Reproducibility and Controversy

Although a number of samples were in good agreement with the results expected from theory and models, some others were reported to have a controversial behaviour. First of all, not all the substrates fully resisted to prolonged water contact, as proven by XRD and absorbance measurements. This issue has been attributed to the critical nature of the parylene layer, which has to be almost free of defects to successfully impede infiltrations. Then, electrochemical characterization were not conclusive. In particular, a couple of batches seems to partially question the previous measurements. Three were the observed differences that characterize these samples: (i) a strong instability in the value of the OCP, that almost prevent from proceeding with the electrochemical measurements; (ii) a substantial (hundreds of mV) potential drop experienced by the photovoltage curve once the LED was turned on, both for substrates coated with SPIRO (Figure 4.18) and coated with PCBM (Figure 4.19); (iii) a larger value of the photocurrent during illumination despite the presence of the same insulating layer. These discrepancies make reproducibility concerns emerge. In effect, despite the important advantages that custom fabrication owns, the reproducibility of samples is typically limited. Many factors in the working conditions affect the quality of the perovskite film. Among these, the working temperature, the working degree of humidity, contaminations, and human errors are the principal responsible for possible degradation of the crystal quality. Although XRD and absorbance measurements did not show substantial differences from the other samples, the extreme instability of the OCP value was taken as a sign of bad quality and high presence of crystal defects. Therefore, the measurements involving this kind of samples were considered unreliable. However, the photovoltage and photocurrent measurements were in any case analyzed to possibly understand the consequences of this inhomogeneity in the sample behaviour. For example, it has been noticed that the samples with no OSC layer present the same three aforementioned alarming characteristics. This confirms that the unexpected behaviour has its origins in the perovskite crystal. In the first instance, ion migration has been identified as the possible responsible. However, it has been observed that the potential drop (ii) is strongly dependent on light-intensity (Figure 4.20). Surprisingly, this would be in contrast with the theory according to which ion conduction inside perovskite crystals is independent of the intensity of light, but only dependent of local generation of electric fields. Thus, if the (ii) and (iii) observed trends are truly related to vacancies and defects, this can suggest that the quantity of photogenerated carriers (given by the intensity of light) seriously affects ion conduction. Yet, many endeavours and future inspections have to be made before reaching hasty conclusions.

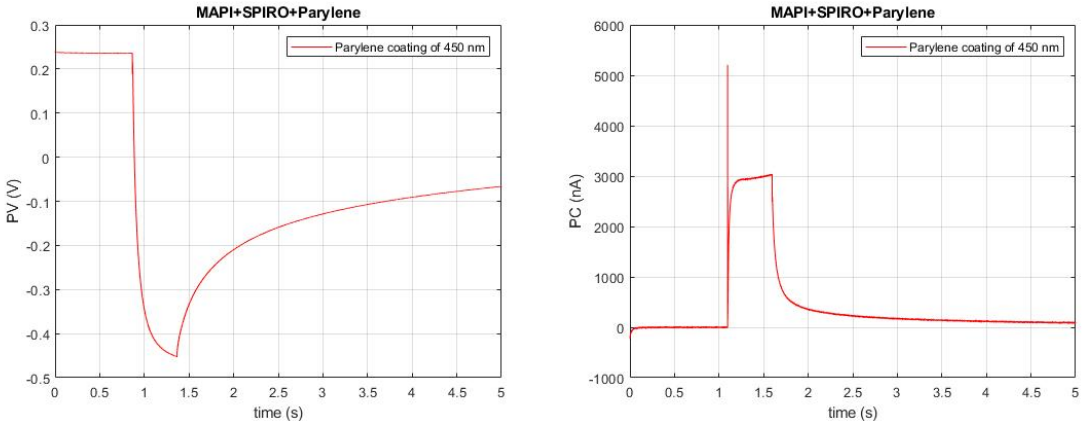

Figure 4.18. Photovoltage and photocurrent measurements of one of the suspected substrates (SPIRO).

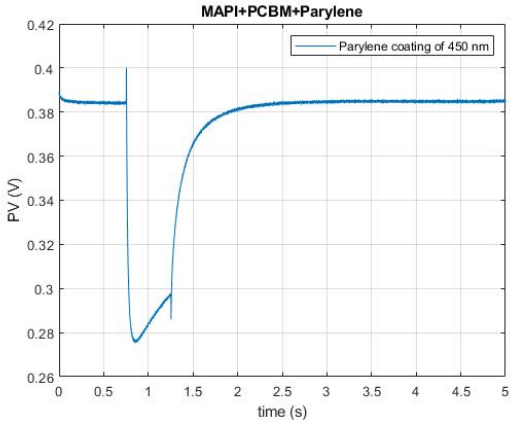

Figure 4.19. Contrary to what was observed in previous samples, this SPIRO substrate presents a significant drop of potential during illumination, similar to the one incurred by the SPIRO substrates. Other samples experienced similar behaviour.

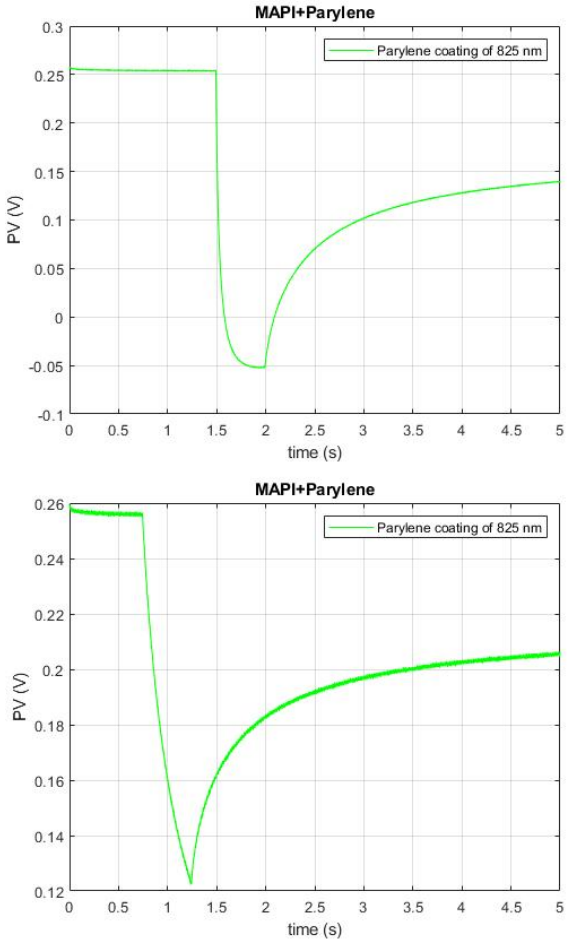

Figure 4.20. The same only-MAPI substrate has been exposed with 100% (on the top) and 30% (on the bottom) light intensity in a photovoltage experiment. The potential drop is clearly cut when the intensity gets lower.

Conclusions

The final purpose of this thesis work was to move some steps towards the understanding of the light-driven stimulation of living cells without the use of invasive nor detrimental methods. In this direction, the realization of efficient semiconductor-based phototransducers for light stimuli would be an important milestone.
First of all, a perovskite archetype crystal ($MAPbI_3$) has been employed as the raw material for the preparation of solar cell-like substrate. Although its outstanding optical properties, this choice of material implied the need of a safe and reliable encapsulation. This study has proven that chemical vapor deposition of Parylene C could be a promising alternative to standard passivation techniques. The former is ideally suitable for biointerface applications since it complies ISO and FDA standards of biocompatibility. The validating tests applied to the samples coated with a conformal layer of polymer have demonstrated a particular resistance of samples to air and water despite the fragile nature of perovskite crystals and organic semiconductors. XRD and absorbance spectrum measurements were conducted before and after the tests as a validating proof. Importantly, the parylene thickness seems not to be a crucial parameter in the protective action against external agents. While, the compactness and the uniformity of the coating has been shown to be the key for a successful encapsulation.
Once the encapsulation of the photoabsorbing substrates was deemed satisfactory, the way to the photostimulation of cells was traced. Electrochemistry measurements have been conducted to simulate the response of the system in a physiological environment. This step is important to understand the optoelectronic behaviour of the substrates when in contact with an electrolyte. Both SPIRO and PCBM coated samples were analyzed. The two were expected to have an opposite behaviour in terms of the sign of the charged carrier extracted that should have been reflected in the electrochemical observations. Photovoltage, Photocurrent and Cyclic Voltammetry measurements were acquired by means of a custom setup made of a LED and an electrochemical cell. These measurements have uniquely shown the presence of a peaked electronic response at the light switching moments, suggesting a capacitive charging and discharging behaviour. At the same time, the steady state behaviour of the system seems not to be completely cut down by the insulating action of the parylene. Moreover, the CV experiments have proven an increased conductivity of the system in the light-ON condition.
An equivalent circuit model has been also developed to properly interpret the results from electrochemistry. Transient simulations performed with LTspice have been conducted to replicate the experimental conditions and validate the model proposed. The model succeeded in predicting the capacitive peaks both in SPIRO and PCBM

coated substrates, suggesting that the electrical properties of the insulation layer are the controlling parameters for such behaviour. Besides, the different sign of the steady state photovoltage has been predicted, and hence attributed to faradaic processes occurring at the interface with the electrolyte. However, as far as concerns this last aspect, controversial experiments were collected. Some samples showed an unexpected drop of potential whose sign is not sensitive to the difference of the charge extraction layer. These batches of samples presented alarming features that make them to be suspected of poor manufacturing quality. Hence, the cited behaviour could be attributed to high density of defects and subsequent ion migration. Some other features seem to confirm the last hypothesis, but the dependence of the size of this effect on light intensity is in contrast with the recognized features of ion migration, which should only depend on the amplitude of local electric fields. Future working is needed to clarify these reproducibility issues.
The natural evolution of this study is the approach to cell culture and the *in-vitro* tests to validate the compatibility of the explored substrates with life. Then, the eventual response of cells to the optoelectronic coupling provided by such substrates has to be further studied and interpreted. This future activity will hopefully shed light on the coupling mechanisms of cell excitation related to the plasma membrane.
At the end, this thesis work provides some insights on the field of research related to photostimulation, which indeed requires a broad multidisciplinary approach and punctual knowledge in different subjects. Then, the presentation of the ongoing experimental activity is brought as one example of the methods employed to move towards the exploitation of this promising technique. The potentiality of the interaction between light and living tissues is still to be properly exploited and will surely give great results to society in the very next future.

Bibliography

[1] B. Hendry, *Membrane physiology and cell excitation*. Springer Science & Business Media, 2013.

[2] V. Vurro, "Non genetic optostimulation for biohybrid light-controlled actuator," 2021.

[3] J. Hopkins, L. Travaglini, A. Lauto, T. Cramer, B. Fraboni, J. Seidel, and D. Mawad, "Photoactive organic substrates for cell stimulation: progress and perspectives," *Advanced Materials Technologies*, vol. 4, no. 5, p. 1800744, 2019.

[4] A. K. Jena, A. Kulkarni, and T. Miyasaka, "Halide perovskite photovoltaics: background, status, and future prospects," *Chemical reviews*, vol. 119, no. 5, pp. 3036–3103, 2019.

[5] T. A. Berhe, W.-N. Su, C.-H. Chen, C.-J. Pan, J.-H. Cheng, H.-M. Chen, M.-C. Tsai, L.-Y. Chen, A. A. Dubale, and B.-J. Hwang, "Organometal halide perovskite solar cells: degradation and stability," *Energy & Environmental Science*, vol. 9, no. 2, pp. 323–356, 2016.

[6] F. C. Krebs, "Fabrication and processing of polymer solar cells: A review of printing and coating techniques," *Solar energy materials and solar cells*, vol. 93, no. 4, pp. 394–412, 2009.

[7] L. J. Phillips, A. M. Rashed, R. E. Treharne, J. Kay, P. Yates, I. Z. Mitrovic, A. Weerakkody, S. Hall, and K. Durose, "Maximizing the optical performance of planar ch3nh3pbi3 hybrid perovskite heterojunction stacks," *Solar Energy Materials and Solar Cells*, vol. 147, pp. 327–333, 2016.

[8] F. Ebadi, M. Aryanpour, R. Mohammadpour, and N. Taghavinia, "Coupled ionic-electronic equivalent circuit to describe asymmetric rise and decay of photovoltage profile in perovskite solar cells," *Scientific reports*, vol. 9, no. 1, pp. 1–9, 2019.

[9] H. Kang, G. Kim, J. Kim, S. Kwon, H. Kim, and K. Lee, "Bulk-heterojunction organic solar cells: Five core technologies for their commercialization," *Advanced Materials*, vol. 28, no. 36, pp. 7821–7861, 2016.

[10] F. Di Maria, F. Lodola, E. Zucchetti, F. Benfenati, and G. Lanzani, "The evolution of artificial light actuators in living systems: from planar to nanostructured interfaces," *Chemical Society Reviews*, vol. 47, no. 13, pp. 4757–4780, 2018.

[11] G. Lanzani, "Organic electronics meets biology," *Nature materials*, vol. 13, no. 8, pp. 775–776, 2014.

[12] C. E. Larson and E. Meng, "A review for the peripheral nerve interface designer," *Journal of neuroscience methods*, vol. 332, p. 108523, 2020.

[13] S. Nag and N. V. Thakor, "Implantable neurotechnologies: electrical stimulation and applications," *Medical & biological engineering & computing*, vol. 54, no. 1, pp. 63–76, 2016.

[14] R. Fettiplace and D. Haydon, "Water permeability of lipid membranes." *Physiological Reviews*, vol. 60, no. 2, pp. 510–550, 1980.

[15] N. Martino, P. Feyen, M. Porro, C. Bossio, E. Zucchetti, D. Ghezzi, F. Benfenati, G. Lanzani, and M. R. Antognazza, "Photothermal cellular stimulation in functional bio-polymer interfaces," *Scientific reports*, vol. 5, no. 1, pp. 1–8, 2015.

[16] M. R. Antognazza, N. Martino, D. Ghezzi, P. Feyen, E. Colombo, D. Endeman, F. Benfenati, and G. Lanzani, "Shedding light on living cells," *Advanced Materials*, vol. 27, no. 46, pp. 7662–7669, 2015.

[17] H. Hirase, V. Nikolenko, J. H. Goldberg, and R. Yuste, "Multiphoton stimulation of neurons," *Journal of neurobiology*, vol. 51, no. 3, pp. 237–247, 2002.

[18] N. Smith, S. Iwanaga, T. Beppu, K. Fujita, O. Nakamura, and S. Kawata, "Photostimulation of two types of ca2+ waves in rat pheochromocytoma pc12 cells by ultrashort pulsed near-infrared laser irradiation," *Laser Physics Letters*, vol. 3, no. 3, pp. 154–161, 2006.

[19] S. Iwanaga, N. Smith, K. Fujita, S. Kawata, and O. Nakamura, "Single-pulse cell stimulation with a near-infrared picosecond laser," *Applied Physics Letters*, vol. 87, no. 24, p. 243901, 2005.

[20] G. Allegre, S. Avrillier, and D. Albe-Fessard, "Stimulation in the rat of a nerve fiber bundle by a short uv pulse from an excimer laser," *Neuroscience letters*, vol. 180, no. 2, pp. 261–264, 1994.

[21] J. Wells, C. Kao, K. Mariappan, J. Albea, E. D. Jansen, P. Konrad, and A. Mahadevan-Jansen, "Optical stimulation of neural tissue in vivo," *Optics letters*, vol. 30, no. 5, pp. 504–506, 2005.

[22] S. M. Rajguru, C.-P. Richter, A. I. Matic, G. R. Holstein, S. M. Highstein, G. M. Dittami, and R. D. Rabbitt, "Infrared photostimulation of the crista ampullaris," *The Journal of physiology*, vol. 589, no. 6, pp. 1283–1294, 2011.

[23] M. W. Jenkins, A. Duke, S. Gu, Y. Doughman, H. Chiel, H. Fujioka, M. Watanabe, E. Jansen, and A. Rollins, "Optical pacing of the embryonic heart," *Nature photonics*, vol. 4, no. 9, pp. 623–626, 2010.

[24] M. G. Shapiro, K. Homma, S. Villarreal, C.-P. Richter, and F. Bezanilla, "Infrared light excites cells by changing their electrical capacitance," *Nature communications*, vol. 3, no. 1, pp. 1–11, 2012.

[25] E. S. Albert, J. M. Bec, G. Desmadryl, K. Chekroud, C. Travo, S. Gaboyard, F. Bardin, I. Marc, M. Dumas, G. Lenaers *et al.*, "Trpv4 channels mediate the infrared laser-evoked response in sensory neurons," *Journal of neurophysiology*, vol. 107, no. 12, pp. 3227–3234, 2012.

[26] H. A. Lester and J. M. Nerbonne, "Physiological and pharmacological manipulations with light flashes," *Annual review of biophysics and bioengineering*, vol. 11, no. 1, pp. 151–175, 1982.

[27] E. M. Callaway and L. C. Katz, "Photostimulation using caged glutamate reveals functional circuitry in living brain slices," *Proceedings of the National Academy of Sciences*, vol. 90, no. 16, pp. 7661–7665, 1993.

[28] J. Noh, R. P. Seal, J. A. Garver, R. H. Edwards, and K. Kandler, "Glutamate co-release at gaba/glycinergic synapses is crucial for the refinement of an inhibitory map," *Nature neuroscience*, vol. 13, no. 2, pp. 232–238, 2010.

[29] Y. Shen, R. Campbell, D. Côté, and M. Paquet, "Challenges for therapeutic applications of opsin-based optogenetic tools in humans." *Frontiers in Neural Circuits*, vol. 14, pp. 41–41, 2020.

[30] K. Deisseroth, "Optogenetics and psychiatry: applications, challenges, and opportunities," *Biological psychiatry*, vol. 71, no. 12, pp. 1030–1032, 2012.

[31] T. C. Pappas, W. S. Wickramanyake, E. Jan, M. Motamedi, M. Brodwick, and N. A. Kotov, "Nanoscale engineering of a cellular interface with semiconductor nanoparticle films for photoelectric stimulation of neurons," *Nano letters*, vol. 7, no. 2, pp. 513–519, 2007.

[32] K. Lugo, X. Miao, F. Rieke, and L. Y. Lin, "Remote switching of cellular activity and cell signaling using light in conjunction with quantum dots," *Biomedical optics express*, vol. 3, no. 3, pp. 447–454, 2012.

[33] M. A. Colicos, B. E. Collins, M. J. Sailor, and Y. Goda, "Remodeling of synaptic actin induced by photoconductive stimulation," *Cell*, vol. 107, no. 5, pp. 605–616, 2001.

[34] J. Rivnay, R. M. Owens, and G. G. Malliaras, "The rise of organic bioelectronics," *Chemistry of Materials*, vol. 26, no. 1, pp. 679–685, 2014.

[35] D. Ghezzi, M. R. Antognazza, M. Dal Maschio, E. Lanzarini, F. Benfenati, and G. Lanzani, "A hybrid bioorganic interface for neuronal photoactivation," *Nature communications*, vol. 2, no. 1, pp. 1–7, 2011.

[36] V. Vurro, A. D. Scaccabarozzi, F. Lodola, F. Storti, F. Marangi, A. M. Ross, G. M. Paternò, F. Scotognella, L. Criante, M. Caironi *et al.*, "A polymer blend substrate for skeletal muscle cells alignment and photostimulation," *Advanced Photonics Research*, vol. 2, no. 2, p. 2000103, 2021.

[37] A. R. Chakhmouradian and P. M. Woodward, "Celebrating 175 years of perovskite research: a tribute to roger h. mitchell," 2014.

[38] H. L. Wells, "Über die cäsium-und kalium-bleihalogenide," *Zeitschrift für anorganische Chemie*, vol. 3, no. 1, pp. 195–210, 1893.

[39] T. Kondo, S. Iwamoto, S. Hayase, K. Tanaka, J. Ishi, M. Mizuno, K. Ema, and R. Ito, "Resonant third-order optical nonlinearity in the layered perovskite-type material (c6h13nh3) 2pbi4," *Solid state communications*, vol. 105, no. 8, pp. 503–506, 1998.

[40] J. Ishi, M. Mizuno, H. Kunugita, K. Ema, S. Iwamoto, S. Hayase, T. Kondo, and R. Ito, "Third-order optical nonlinearity due to excitons and biexcitons in a self-organized quantum-well material (c6h13nh3) 2pbi4," *Journal of Nonlinear Optical Physics & Materials*, vol. 7, no. 01, pp. 153–159, 1998.

[41] A. Kojima, K. Teshima, Y. Shirai, and T. Miyasaka, "Novel photoelectrochemical cell with mesoscopic electrodes sensitized by lead-halide compounds (5)," in *ECS Meeting Abstracts*, no. 8. IOP Publishing, 2007, p. 352.

[42] Z. Yi, N. H. Ladi, X. Shai, H. Li, Y. Shen, and M. Wang, "Will organic–inorganic hybrid halide lead perovskites be eliminated from optoelectronic applications?" *Nanoscale Advances*, vol. 1, no. 4, pp. 1276–1289, 2019.

[43] G. Giorgi, J.-I. Fujisawa, H. Segawa, and K. Yamashita, "Small photocarrier effective masses featuring ambipolar transport in methylammonium lead iodide perovskite: a density functional analysis," *The journal of physical chemistry letters*, vol. 4, no. 24, pp. 4213–4216, 2013.

[44] C. C. Boyd, R. Cheacharoen, T. Leijtens, and M. D. McGehee, "Understanding degradation mechanisms and improving stability of perovskite photovoltaics," *Chemical reviews*, vol. 119, no. 5, pp. 3418–3451, 2018.

[45] J. A. Christians, P. A. Miranda Herrera, and P. V. Kamat, "Transformation of the excited state and photovoltaic efficiency of ch3nh3pbi3 perovskite upon controlled exposure to humidified air," *Journal of the American Chemical Society*, vol. 137, no. 4, pp. 1530–1538, 2015.

[46] U. B. Cappel, T. Daeneke, and U. Bach, "Oxygen-induced doping of spiro-meotad in solid-state dye-sensitized solar cells and its impact on device performance," *Nano letters*, vol. 12, no. 9, pp. 4925–4931, 2012.

[47] A. J. Pearson, G. E. Eperon, P. E. Hopkinson, S. N. Habisreutinger, J. T.-W. Wang, H. J. Snaith, and N. C. Greenham, "Oxygen degradation in mesoporous al2o3/ch3nh3pbi3-xclx perovskite solar cells: kinetics and mechanisms," *Advanced Energy Materials*, vol. 6, no. 13, p. 1600014, 2016.

[48] N. Aristidou, C. Eames, I. Sanchez-Molina, X. Bu, J. Kosco, M. S. Islam, and S. A. Haque, "Fast oxygen diffusion and iodide defects mediate oxygen-induced degradation of perovskite solar cells," *Nature communications*, vol. 8, no. 1, pp. 1–10, 2017.

[49] M. M. Lee, J. Teuscher, T. Miyasaka, T. N. Murakami, and H. J. Snaith, "Efficient hybrid solar cells based on meso-superstructured organometal halide perovskites," *Science*, vol. 338, no. 6107, pp. 643–647, 2012.

[50] D. W. DeQuilettes, W. Zhang, V. M. Burlakov, D. J. Graham, T. Leijtens, A. Osherov, V. Bulović, H. J. Snaith, D. S. Ginger, and S. D. Stranks, "Photo-induced halide redistribution in organic–inorganic perovskite films," *Nature communications*, vol. 7, no. 1, pp. 1–9, 2016.

[51] G. Y. Kim, A. Senocrate, T.-Y. Yang, G. Gregori, M. Grätzel, and J. Maier, "Large tunable photoeffect on ion conduction in halide perovskites and implications for photodecomposition," *Nature materials*, vol. 17, no. 5, pp. 445–449, 2018.

[52] Y. Luo, P. Khoram, S. Brittman, Z. Zhu, B. Lai, S. P. Ong, E. C. Garnett, and D. P. Fenning, "Direct observation of halide migration and its effect on the photoluminescence of methylammonium lead bromide perovskite single crystals," *Advanced Materials*, vol. 29, no. 43, p. 1703451, 2017.

[53] W. R. Mateker and M. D. McGehee, "Progress in understanding degradation mechanisms and improving stability in organic photovoltaics," *Advanced materials*, vol. 29, no. 10, p. 1603940, 2017.

[54] E. J. Juarez-Perez, Z. Hawash, S. R. Raga, L. K. Ono, and Y. Qi, "Thermal degradation of ch 3 nh 3 pbi 3 perovskite into nh 3 and ch 3 i gases observed by coupled thermogravimetry–mass spectrometry analysis," *Energy & environmental science*, vol. 9, no. 11, pp. 3406–3410, 2016.

[55] A. Uddin, M. B. Upama, H. Yi, and L. Duan, "Encapsulation of organic and perovskite solar cells: A review," *Coatings*, vol. 9, no. 2, p. 65, 2019.

[56] A. da Silva Sobrinho, M. Latreche, G. Czeremuszkin, J. Klemberg-Sapieha, and M. Wertheimer, "Transparent barrier coatings on polyethylene terephthalate by single-and dual-frequency plasma-enhanced chemical vapor deposition," *Journal of Vacuum Science & Technology A: Vacuum, Surfaces, and Films*, vol. 16, no. 6, pp. 3190–3198, 1998.

[57] L. Shi, T. L. Young, J. Kim, Y. Sheng, L. Wang, Y. Chen, Z. Feng, M. J. Keevers, X. Hao, P. J. Verlinden *et al.*, "Accelerated lifetime testing of organic–inorganic perovskite solar cells encapsulated by polyisobutylene," *ACS applied materials & interfaces*, vol. 9, no. 30, pp. 25 073–25 081, 2017.

[58] J. Granstrom, J. Swensen, J. Moon, G. Rowell, J. Yuen, and A. Heeger, "Encapsulation of organic light-emitting devices using a perfluorinated polymer," *Applied physics letters*, vol. 93, no. 19, p. 409, 2008.

[59] V. Parylene, "Vsi parylene brochure – the complete guide to parylene coating." [Online]. Available: https://www.ellsworth.com/globalassets/literature-library/manufacturer/vsi-parylene/vsi-parylene-brochure---the-complete-guide-to-parylene-coatings.pdf

[60] [Online]. Available: https://engineering.tufts.edu/microfab/documents/Parylene.pdf

[61] N. Coron, C. Cuesta, E. García, C. Ginestra, T. A. Girard, P. de Marcillac, M. Martínez, Y. Ortigoza, A. O. de Solórzano, C. Pobes *et al.*, "Response of parylene-coated nai (tl) scintillators at low temperature," in *EPJ Web of Conferences*, vol. 65. EDP Sciences, 2014, p. 02001.

[62] J. B. Fortin and T.-M. Lu, *Chemical vapor deposition polymerization: the growth and properties of parylene thin films*. Springer Science & Business Media, 2003.

[63] J. Ortigoza-Diaz, K. Scholten, C. Larson, A. Cobo, T. Hudson, J. Yoo, A. Baldwin, A. Weltman Hirschberg, and E. Meng, "Techniques and considerations in the microfabrication of parylene c microelectromechanical systems," *Micromachines*, vol. 9, no. 9, p. 422, 2018.

[64] J. Jeong, M. Kim, J. Seo, H. Lu, P. Ahlawat, A. Mishra, Y. Yang, M. A. Hope, F. T. Eickemeyer, M. Kim *et al.*, "Pseudo-halide anion engineering for α-fapbi 3 perovskite solar cells," *Nature*, vol. 592, no. 7854, pp. 381–385, 2021.

[65] J. J. Yoo, G. Seo, M. R. Chua, T. G. Park, Y. Lu, F. Rotermund, Y.-K. Kim, C. S. Moon, N. J. Jeon, J.-P. Correa-Baena *et al.*, "Efficient perovskite solar cells via improved carrier management," *Nature*, vol. 590, no. 7847, pp. 587–593, 2021.

[66] J.-P. Correa-Baena, A. Abate, M. Saliba, W. Tress, T. J. Jacobsson, M. Grätzel, and A. Hagfeldt, "The rapid evolution of highly efficient perovskite solar cells," *Energy & Environmental Science*, vol. 10, no. 3, pp. 710–727, 2017.

[67] Z.-K. Tan, R. S. Moghaddam, M. L. Lai, P. Docampo, R. Higler, F. Deschler, M. Price, A. Sadhanala, L. M. Pazos, D. Credgington *et al.*, "Bright light-emitting diodes based on organometal halide perovskite," *Nature nanotechnology*, vol. 9, no. 9, pp. 687–692, 2014.

[68] X. Yang, X. Zhang, J. Deng, Z. Chu, Q. Jiang, J. Meng, P. Wang, L. Zhang, Z. Yin, and J. You, "Efficient green light-emitting diodes based on quasi-two-dimensional composition and phase engineered perovskite with surface passivation," *Nature communications*, vol. 9, no. 1, pp. 1–8, 2018.

[69] J. Wang, N. Wang, Y. Jin, J. Si, Z.-K. Tan, H. Du, L. Cheng, X. Dai, S. Bai, H. He *et al.*, "Interfacial control toward efficient and low-voltage perovskite light-emitting diodes," *Advanced Materials*, vol. 27, no. 14, pp. 2311–2316, 2015.

[70] R. Dong, Y. Fang, J. Chae, J. Dai, Z. Xiao, Q. Dong, Y. Yuan, A. Centrone, X. C. Zeng, and J. Huang, "Photodetectors: High-gain and low-driving-voltage photodetectors based on organolead triiodide perovskites (adv. mater. 11/2015)," *Advanced Materials*, vol. 27, no. 11, pp. 1967–1967, 2015.

[71] D. Li, G. Dong, W. Li, and L. Wang, "High performance organic-inorganic perovskite-optocoupler based on low-voltage and fast response perovskite compound photodetector," *Scientific reports*, vol. 5, no. 1, pp. 1–6, 2015.

[72] S. Yakunin, Y. Shynkarenko, D. N. Dirin, I. Cherniukh, and M. V. Kovalenko, "Non-dissipative internal optical filtering with solution-grown perovskite single crystals for full-colour imaging," *NPG Asia Materials*, vol. 9, no. 9, pp. e431–e431, 2017.

[73] S. Yakunin, M. Sytnyk, D. Kriegner, S. Shrestha, M. Richter, G. J. Matt, H. Azimi, C. J. Brabec, J. Stangl, M. V. Kovalenko *et al.*, "Detection of x-ray photons by solution-processed lead halide perovskites," *Nature photonics*, vol. 9, no. 7, pp. 444–449, 2015.

[74] W. Wei, Y. Zhang, Q. Xu, H. Wei, Y. Fang, Q. Wang, Y. Deng, T. Li, A. Gruverman, L. Cao *et al.*, "Monolithic integration of hybrid perovskite single crystals with heterogenous substrate for highly sensitive x-ray imaging," *Nature Photonics*, vol. 11, no. 5, pp. 315–321, 2017.

[75] C.-Y. Chen, J.-H. Chang, K.-M. Chiang, H.-L. Lin, S.-Y. Hsiao, and H.-W. Lin, "Perovskite photovoltaics for dim-light applications," *Advanced Functional Materials*, vol. 25, no. 45, pp. 7064–7070, 2015.

[76] X. Hu, F. Li, and Y. Song, "Wearable power source: a newfangled feasibility for perovskite photovoltaics," *ACS Energy Letters*, vol. 4, no. 5, pp. 1065–1072, 2019.

[77] H. Zhang, X. Wang, Q. Liao, Z. Xu, H. Li, L. Zheng, and H. Fu, "Embedding perovskite nanocrystals into a polymer matrix for tunable luminescence probes in cell imaging," *Advanced Functional Materials*, vol. 27, no. 7, p. 1604382, 2017.

[78] Y. Wang, J. He, H. Chen, J. Chen, R. Zhu, P. Ma, A. Towers, Y. Lin, A. J. Gesquiere, S.-T. Wu *et al.*, "Ultrastable, highly luminescent organic–inorganic perovskite–polymer composite films," *Advanced Materials*, vol. 28, no. 48, pp. 10 710–10 717, 2016.

[79] M. M. Aria, S. B. Srivastava, E. Sekerdag, U. M. Dikbas, S. Sadeghi, S. R. Pering, P. J. Cameron, Y. Gursoy-Ozdemir, I. H. Kavakli, and S. Nizamoglu, "Perovskite-based optoelectronic biointerfaces for non-bias-assisted photostimulation of cells," *Advanced Materials Interfaces*, vol. 6, no. 17, p. 1900758, 2019.

[80] M. Konstantakou, D. Perganti, P. Falaras, and T. Stergiopoulos, "Anti-solvent crystallization strategies for highly efficient perovskite solar cells," *Crystals*, vol. 7, no. 10, p. 291, 2017.

[81] G. Chiaravalli, G. Manfredi, R. Sacco, and G. Lanzani, "Photoelectrochemistry and drift–diffusion simulations in a polythiophene film interfaced with an electrolyte," *ACS applied materials & interfaces*, vol. 13, no. 30, pp. 36 595–36 604, 2021.

[82] H. Lee, S. Gaiaschi, P. Chapon, D. Tondelier, J.-E. Bouree, Y. Bonnassieux, V. Derycke, and B. Geffroy, "Effect of halide ion migration on the electrical properties of methylammonium lead tri-iodide perovskite solar cells," *The Journal of Physical Chemistry C*, vol. 123, no. 29, pp. 17 728–17 734, 2019.

[83] J. E. B. Randles, "Kinetics of rapid electrode reactions," *Discussions of the faraday society*, vol. 1, pp. 11–19, 1947.

[84] J.-U. Chu, K.-I. Song, A. Shon, S. Han, S. H. Lee, J. Y. Kang, D. Hwang, J.-K. F. Suh, K. Choi, and I. Youn, "Feedback control of electrode offset voltage during functional electrical stimulation," *Journal of neuroscience methods*, vol. 218, no. 1, pp. 55–71, 2013.